Monitoring and manipulation of vacuum-induced coherences in frequency-resolved correlation

He-bin Zhang, Shao-ping Wu, and Gao-xiang Li*
Department of Physics, Huazhong Normal University, Wuhan 430079, China

(Received 18 May 2020; accepted 2 November 2020; published 17 November 2020)

The frequency-resolved correlations of the fluorescence emitted by a four-level system in the $J = 1/2$ to $J = 1/2$ transition driven by a linearly polarized laser field are theoretically investigated. In the cross two-photon correlation of the π and σ^+ transitions, we show that VICs can induce the interference of time orderings between the two-photon paths with different dipole moments, which can serve as a good scheme to exhibit the effects of vacuum-induced coherences (VICs). An external magnetic field can cause frequency differences between two-photon paths with different time orderings. When the differences can be distinguished by detectors, the effects of VICs are destroyed and time asymmetry of the two-photon correlations appears due to the reveal of "which path" information. However, the which path information can be erased by tuning the filtering frequencies so the perfect interference effects of time orderings and time symmetry are restored.

DOI: 10.1103/PhysRevA.102.053717

I. INTRODUCTION

Vacuum was always viewed as the origin of the destruction of the quantum coherence intuitively until the effects of vacuum-induced coherences (VICs) were first proposed and discussed in the V-shaped system [1,2]. Subsequently, a large number of effects caused by VICs were reported in V-shaped and Λ-shaped systems, such as ultrasharp spectral lines [3], enhancement of squeezing [4,5], and lasing without inversion [6]. Relevant progress in experiments is being made [7–10] and VICs have been observed in multiple platforms, such as a single InGaAs quantum dot [8], and an ensemble of ^{57}Fe nuclei [9]. Unfortunately, it is considered quite difficult to meet the conditions for the appearance of VICs in real atomic systems, which involve a variety of important platforms in the fields of quantum technologies such as cold atoms, trapped ions, and atomic gases, and thus there is rarely related experimental observation reported in these systems. Meanwhile, Evers *et al.* [11] and Agarwal *et al.* [12] proposed theory schemes for monitoring the effects of VICs contained in the fluorescence emitted by a four-level system in the $J = 1/2$ to $J = 1/2$ transition which is realizable, for example, in trapped $^{198}Hg^+$ [13] and $^{138}Ba^+$ [14,15] ions. Nevertheless, the corresponding experimental implementation has not been reported yet. Worth noting, in contrast to the various effects of VICs found in the three-level systems [3–6], more and further studies on VICs based on this four-level system are needed to exploit the potential of VICs as a quantum resource with a noticeable robustness in real environments.

On the other hand, the photon correlation has been a central quantity in quantum optics since it was proposed by Glauber [16,17]. As an extension of the frequency-blind correlation which only reflects the overall statistical property of the radiation field, the frequency-resolved correlation [18–21] reveals the correlations between specific spectral components and then can provide deeper insight into the statistical property of emitted radiation. Due to the rapid development of quantum technologies, the frequency-resolved correlation has received renewed attention in recent years, and the correlations only between the spectral peaks are extended to all the possible frequencies [22,23], which greatly facilitates research on the frequency-resolved correlation. The relevant research proves that the frequency-resolved correlation is a treasure. A variety of nontrivial phenomena in quantum optics contained in spectral components of fluorescence were revealed, such as anticorrelations [24], the violation of classical inequalities [25–27], and the effects of antibunching and bunching [23,28], and new schemes of quantum sources were proposed [25–29], such as single-photon sources, two-photon sources, and source of entangled photon pairs.

In contrast to the abundant quantum effects revealed, the frequency-filtered correlation measurement scheme can be conveniently implemented experimentally by inserting filters between the emitter and the broadband detectors [30–35]. Naturally, related experimental research has developed rapidly in recent years [24–26,36–39]. For instance, Muller *et al.* [25] reported the measurement of the two-photon spectrum, and observed successfully the violation of Cauchy-Schwarz inequality and the strong photon correlations originated from the so-called leapfrog processes predicted in Refs. [23,28]. Noticeably, it was proved recently [26] that entangled photon pairs can be generated via the external frequency-filtered manipulation of the resonance fluorescence from a two-level quantum dot. This work confirms a new way to generate entangled photon pairs besides parametric process [40,41] and cascaded emission in a multilevel atom [42] or a biexciton structure of a quantum dot [31,43].

Considering the advantages in revealing and analyzing quantum optical effects contained in the spectral components of fluorescence and the potential in manipulating emitted radiation, we try utilizing the frequency-resolved correlation to

*gaox@mail.ccnu.edu.cn

explore the expected effects of VICs contained in fluorescence. In addition, we know that the destruction on quantum coherence caused by vacuum reservoir is often viewed as a main obstacle that needs to be overcome in the field of quantum technologies. VICs, however, indicate that vacuum reservoir can induce quantum coherence and then lead to a variety of interesting effects [3–6]. Therefore, this coherence can serve as a potential quantum resource with good performance in manipulation and robustness in real environments. Given this, it is only the first step to monitor VICs under ideal measurement conditions, such as the infinite resolution in frequency or time [11,12]. Furthermore, it is worth exploring the performance of VICs on a more general optical target. In fact, the optical target with a finite frequency resolution is always encountered in quantum information applications such as distance quantum communication [44], optical quantum computation [45], and solid-state quantum networks [46,47]. Therefore, there is considerable interest to explore how to reveal and even manipulate VICs by the optical target under the above conditions.

In this paper, we follow the theoretical method developed in Ref. [22] for the frequency-resolved correlation, where, to simulate the filtering process, quantized sensors are included in a theoretical model. The application of this method can make the calculations of the frequency-resolved correlation straightforward and simple because complicated convolution can be avoided. Besides the frequency filter, the sensor can also be theoretically viewed as a detector or even a general optical target with a finite linewidth in the field of quantum technologies, so the investigations on the detection and the manipulation of the emitted radiation can also be involved based on this theoretical method. Therefore, the purpose of this paper is not only to propose a new scheme to monitor VICs based on the frequency-filtered correlation measurement, but also to explore the possibilities of monitoring directly and even manipulating this potential quantum source by the optical target with a finite linewidth.

The possibility to research effects of VICs in the $J = 1/2$ to $J = 1/2$ transition of a real atomic system is indicated in Refs. [11,12]. For a further investigation, we also choose the $J = 1/2$ to $J = 1/2$ transition as the quantum emitter and analyze the frequency-resolved correlations between the π and σ^+ transitions mainly in the large detection linewidth and strong excitation regime. We demonstrate that VICs can induce the interference between different time orderings of emission with different combinations of dipole moments, and this kind of physical origin is significantly different from that in the conventional interference of time orderings [48,49]. To be specific, in the conventional interference of time orderings, the two two-photon paths involved originate from the same dipole moment in the two-level system [48] or the same combination of dipole moments in the multilevel system [49]. However, in this paper, the two two-photon paths involved are based on different combinations of dipole moments, between which the interference is induced by VICs arising between the two spontaneous decay channels of the π transitions. In the absence of VICs, the above-mentioned interference of time orderings would not appear. Next, we find that the external magnetic field can cause a frequency difference between the specific coherent two-photon transition paths. When the frequency difference can be distinguished by the detector, "which path" information of the two-photon transitions is revealed, which can cause the interference between different time orderings of emission induced by VICs to disappear and the time symmetry of the correlation once appearing in the case of degenerate system to be broken. However, inspired by Refs. [28,31,50–52], we demonstrate that which path information can be erased by the external manipulation of filters, so the perfect interference of time orderings and the time symmetry of the correlation can recover again.

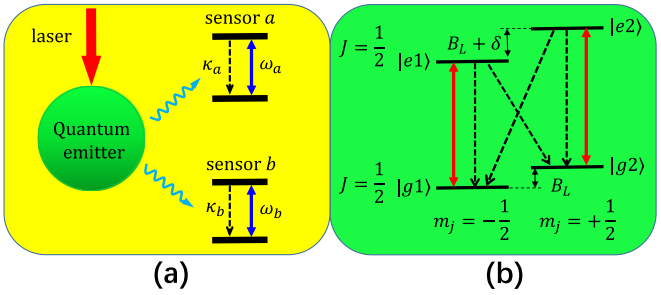

FIG. 1. (a) Schematic diagram of the coupling between the quantum emitter and sensors. Each sensor is represented by a two-level system with the annihilation operator [22] and can simulate the filtering and detection processes. According to the sensor method, the frequency-resolved correlations of the emitted photons can be computed conveniently. (b) Level scheme of the $J = 1/2$ to $J = 1/2$ transition. The transitions $|e_1\rangle \leftrightarrow |g_1\rangle$ and $|e_2\rangle \leftrightarrow |g_2\rangle$ driven by a π polarized laser, and the external static magnetic field in the direction of the quantization axis can cause the Zeeman splitting of the magnetic sublevels.

The paper is organized as follows. In Sec. II, the theoretical model of the system is introduced. In Sec. III, we analyze the different spectral components of the two-photon transitions consisting of the σ^+ and π transitions and obtain the general analytical expression of the frequency-resolved correlation between all possible frequencies. In Sec. IV, we specifically discuss the two-photon correlation function at zero and nonzero delays in the case of degenerate system and note that the interference between different time orderings of emission induced by VICs can be clearly indicated. Then, in the case of nondegenerate system, the influences of an external magnetic field and the manipulation of filters on the interference effects of time orderings are explored. The last section is a summary.

II. THEORETICAL MODEL

We consider a $J = 1/2$ to $J = 1/2$ transition driven by a linearly polarized laser of the frequency ω as the quantum emitter. The level scheme is shown in Fig. 1(b) and can be achieved, for example, in the $6s\,^2S_{1/2}$–$6p\,^2P_{1/2}$ transition of trapped $^{198}Hg^+$ [13] and $^{138}Ba^+$ [14,15] ions. It can be seen that the emitted (or absorbed) photon is π polarized in the transitions $|e_1\rangle \leftrightarrow |g_1\rangle$ and $|e_2\rangle \leftrightarrow |g_2\rangle$, σ^+ polarized in the transition $|e_2\rangle \leftrightarrow |g_1\rangle$, and σ^- polarized in the transition $|e_1\rangle \leftrightarrow |g_2\rangle$. The quantization axis (z axis) is set along the polarization direction of the laser, and then only the π transitions $|e_1\rangle \leftrightarrow |g_1\rangle$ and $|e_2\rangle \leftrightarrow |g_2\rangle$ are driven. Within the rotating

wave approximation, the Hamiltonian of the quantum emitter in the frame rotating at the driving laser frequency can be given by

$$H_\sigma = -\left[\Delta\sigma_{e_1e_1} + (\Delta-\delta)\sigma_{e_2e_2} - B_L\left(\sigma_{e_2e_2}+\sigma_{g_2g_2}\right)\right] + \left(V_{e_1g_1}\sigma_{e_1g_1} + V_{e_2g_2}\sigma_{e_2g_2} + \text{H.c.}\right). \quad (1)$$

Here the transition operators are defined as $\sigma_{mn} \equiv |m\rangle\langle n|$. $\Delta = \omega_1 - \omega_L$ is the detuning of the transition $|e_1\rangle \leftrightarrow |g_1\rangle$ frequencies from the laser and ω_1 represents the resonance frequency of the transition $|e_1\rangle \leftrightarrow |g_1\rangle$. $V_{e_1g_1}$ and $V_{e_2g_2}$, respectively, represent the Rabi frequencies of the transitions $|e_1\rangle \leftrightarrow |g_1\rangle$ and $|e_2\rangle \leftrightarrow |g_2\rangle$, and we can define $\Omega = V_{e_1g_1} = -V_{e_2g_2}$ according to Appendix. A. Since the magnetic quantum numbers of the four sublevels are nonzero, the external static magnetic field in the direction of the quantization axis can cause a frequency splitting B_L between the sublevels with different magnetic quantum numbers. In addition, due to the difference between the Landé g factors of the ground state and the excited state, a splitting δ between the transition frequencies of $|e_1\rangle \leftrightarrow |g_1\rangle$ and $|e_2\rangle \leftrightarrow |g_2\rangle$ occurs.

The time evolution of the quantum emitter is governed by the master equation

$$\dot{\rho_\sigma} = -i[H_\sigma, \rho_\sigma] + \mathcal{L}_\sigma\rho_\sigma, \quad (2)$$

where the dissipation term $\mathcal{L}_\sigma\rho_\sigma$ of the emitter takes the form

$$\mathcal{L}_\sigma\rho_\sigma = \frac{\gamma_1}{2}D\left[\sigma_{g_1e_1}\right]\rho_\sigma + \frac{\gamma_2}{2}D\left[\sigma_{g_2e_2}\right]\rho_\sigma + \frac{\gamma_3}{2}D\left[\sigma_{g_2e_1}\right]\rho_\sigma + \frac{\gamma_4}{2}D\left[\sigma_{g_1e_2}\right]\rho_\sigma + \frac{\gamma_{21}}{2}\left(2\sigma_{g_2e_2}\rho_\sigma\sigma_{e_1g_1}\right) + \frac{\gamma_{12}}{2}\left(2\sigma_{g_1e_1}\rho_\sigma\sigma_{e_2g_2}\right). \quad (3)$$

Here the first four terms denote the spontaneous decay of the system with the Lindblad superoperator $D[\sigma_{mn}]\rho \equiv 2\sigma_{mn}\rho\sigma_{nm} - \rho\sigma_{nm}\sigma_{mn} - \sigma_{nm}\sigma_{mn}\rho$ $(m, n = g_1, g_2, e_1, e_2)$. The last two terms origin from the vacuum-induced interference due to the nonorthogonal dipole moments of the two transitions $|e_1\rangle \to |g_1\rangle$ and $|e_2\rangle \to |g_2\rangle$. According to Appendix A, we have $\gamma_1 = \gamma_2 = \gamma/3, \gamma_3 = \gamma_4 = 2\gamma/3, \gamma_{12} = \gamma_{21} = -\gamma/3$, where γ represents total spontaneous decay rate of the transition $J = 1/2$ to $J = 1/2$.

In this paper, we use the so-called sensor method proposed by Ref. [22] to investigate the frequency-resolved correlations of the quantum emitter. Accordingly, the Hamiltonian term $\sum_i H_{s_i}$ and the dissipation term $\sum_i \mathcal{L}_{\kappa_i}\rho$ describing the sensors are added to the original main equation of the emitter system, and the number of sensors depends on the order of the correlation functions. The Hamiltonian of each sensor is $H_{s_i} = \omega_{s_i}a_{s_i}^\dagger a_{s_i} + (ga_{s_i}^\dagger\sigma_{A_i} + \text{H.c.})$, where the first term represents the free Hamiltonian and the second term represents the interaction between the sensors and quantum emitter. a_{s_i} is the annihilation operator of the sensor, ω_{s_i} is the free frequency which can be set to match the emission frequency to be measured, σ_{A_i} represents the transition operator of the emitter coupled to sensor a_{s_i}, and g is the coupling coefficient. The dissipation of each sensor is in Lindblad form $\mathcal{L}_{\kappa_i}\rho_s = \kappa_i D[a_{s_i}]\rho_s$. The decay rate κ_i of the sensor determines the frequency resolution (κ_i) and then the time resolution (κ_i^{-1}), which reflects that the time and frequency cannot be measured with arbitrary precision simultaneously.

Specifically, we mainly focus on the case where two sensors (labeled by the annihilation operators a, b) couple to σ^+ and π-polarized components of the emitted radiation, respectively, in this paper. The schematic diagram of the combined system is shown in Fig. 1(a). Therefore, the corresponding Hamiltonian describing the sensors and their coupling to the emitter in the frame rotating at the driving laser frequency is given by

$$H_s = \Delta_a a^\dagger a + \Delta_b b^\dagger b + \left(g_\sigma\sigma_{e_2g_1}a + \text{H.c.}\right) + \left(g_{\pi_1}\sigma_{e_1g_1}b + g_{\pi_2}\sigma_{e_2g_2}b + \text{H.c.}\right), \quad (4)$$

where $\Delta_a = \omega_a - \omega_L$ and $\Delta_b = \omega_b - \omega_L$ represent the detunings between the sensors and the laser. It should be noted that since the π transitions contains two components $|e_1\rangle \to |g_1\rangle$ and $|e_2\rangle \to |g_2\rangle$, these two transitions couple to sensor b simultaneously. Moreover, since the dipole moments of the two π transitions are antiparallel, their coupling coefficients with sensor b are of opposite signs, i.e., $g_{\pi_2} = -g_{\pi_1}$. The corresponding dissipation term $\mathcal{L}_s\rho$ takes the form

$$\mathcal{L}_s\rho_s = \kappa_a D[a]\rho_s + \kappa_b D[b]\rho_s. \quad (5)$$

Therefore, the master equation of the combined system composed of the quantum emitter and the sensors can be obtained:

$$\dot{\rho} = -i[H_\sigma + H_s, \rho] + \mathcal{L}_\sigma\rho + \mathcal{L}_s\rho. \quad (6)$$

Here $\rho = \sum_{\psi,\phi}\langle\psi|\rho|\phi\rangle|\psi\rangle\langle\phi|$ is the density operator of the combined system, where $|\psi\rangle, |\phi\rangle = |m\rangle \otimes |n_a\rangle \otimes |n_b\rangle$ are the basis states in the Hilbert space of the combined system, ($|m\rangle$ is the state of the emitter, and $|n_a\rangle, |n_b\rangle$ are the number states of sensors a and b, respectively). Theoretically, the role of the sensor can be considered from two aspects. On the one hand, the sensor can model the filter which is theoretically specified by the central frequency and linewidth, and the light emitted by the quantum emitter can be filtered and manipulated by adjusting these two parameters of the filter. On the other hand, the sensor can also be viewed as a simple quantized model of the detector, and therefore the emitter and detector are both involved in the combined system as quantized objects, which ensures that the uncertainty principle is intrinsically accounted for in the theoretical model applied here.

Following the formalism in Ref. [22], the cross-frequency-resolved two-photon correlation of σ^+ and π transitions reads

$$g^{(2)}(\omega_a, \omega_b, \tau) = \frac{\mathcal{G}^{(2)}(\omega_a, \omega_b, \tau)}{\langle n_a(t)\rangle\langle n_b(t+\tau)\rangle}, \quad (7)$$

where $\mathcal{G}^{(2)}(\omega_a, \omega_b, \tau) = \langle a^\dagger(t)b^\dagger(t+\tau)b(t+\tau)a(t)\rangle$ is the unnormalized two-photon correlation function and $n_\varsigma(t) = \varsigma^\dagger(t)\varsigma(t)$ is the population operator of the sensor.

III. GENERAL SOLUTION FOR MASTER EQUATION

First, we point out two concepts which are often involved in the frequency-filtered correlation measurement, that is, the time ordering of emission and the time ordering of detection. The time ordering of emission is the actual order of the physical process happening in the quantum emitter and the

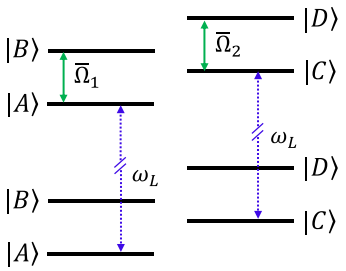

FIG. 2. The dressed-state diagram of the level scheme shown in Fig. 1(b). The two transitions $|e_1\rangle \leftrightarrow |g_1\rangle$ and $|e_2\rangle \leftrightarrow |g_2\rangle$ driven by the π polarized laser, respectively, correspond to the effective Rabi frequencies $\bar{\Omega}_1$ and $\bar{\Omega}_2$.

time ordering of detection is set by the observer. The conventional frequency-blind correlation corresponds to the case where the detection linewidth is infinite, and then these two kind of time orderings are generally consistent in this case. However, the finite linewidth can give rise to an indeterminacy in the time resolution of detection according to the time-energy uncertainty relation. Therefore, in a frequency-filtered correlation measurement, different time orderings of emission may contribute to a certain time ordering of detection if the time difference of successive emission events is less than this indeterminacy.

A. Dressed-state representation

In this paper, we mainly focus on the parameter condition $\Omega \gg \kappa_i \gg \gamma$ applied in Ref. [48], and we temporarily assume $\kappa_i = \kappa$ in the following discussion. Therefore, to explore the origin of the correlation process conveniently, we can introduce the dressed-state representation of the quantum emitter. The dressed states shown in Fig. 2, defined as the eigenstates of the emitter Hamiltonian H_σ, are given by [3]

$$\begin{aligned}
|A\rangle &= c_1|g_1\rangle - e^{i\phi}s_1|e_1\rangle,\\
|B\rangle &= e^{-i\phi}s_1|g_1\rangle + c_1|e_1\rangle,\\
|C\rangle &= c_2|g_2\rangle + e^{i\phi}s_2|e_2\rangle,\\
|D\rangle &= -e^{-i\phi}s_2|g_2\rangle + c_2|e_2\rangle,
\end{aligned} \tag{8}$$

where $c_1 = \cos\theta_1 = \sqrt{\frac{\bar{\Omega}_1-\Delta}{2\bar{\Omega}_1}}$, $s_1 = \sin\theta_1 = \sqrt{\frac{\bar{\Omega}_1+\Delta}{2\bar{\Omega}_1}}$, $c_2 = \cos\theta_2 = \sqrt{\frac{\bar{\Omega}_2-(\Delta-\delta)}{2\bar{\Omega}_2}}$, $s_2 = \sin\theta_2 = \sqrt{\frac{\bar{\Omega}_2+(\Delta-\delta)}{2\bar{\Omega}_2}}$. The effective Rabi frequency $\bar{\Omega}_1 = \sqrt{\Delta^2 + 4|\Omega|^2}$ is the splitting between the neighboring dressed states $|a\rangle$ and $|b\rangle$, and the effective Rabi frequency $\bar{\Omega}_2 = \sqrt{(\Delta-\delta)^2 + 4|\Omega|^2}$ is the splitting between the neighboring dressed states $|c\rangle$ and $|d\rangle$. In the strong excitation regime, the Rabi frequencies satisfy $\bar{\Omega}_1, \bar{\Omega}_2 \gg \gamma$, therefore the different dressed states can be well distinguished. The energies of the dressed states in Eq. (8) can be expressed, respectively, as

$$\begin{aligned}
E_A &= (-\Delta - \bar{\Omega}_1)/2,\\
E_B &= (-\Delta + \bar{\Omega}_1)/2,\\
E_C &= (2B + \delta - \Delta - \bar{\Omega}_2)/2,\\
E_D &= (2B + \delta - \Delta + \bar{\Omega}_2)/2.
\end{aligned} \tag{9}$$

The transition operators of the emitter in the bare-state representation can be decomposed into the following forms:

$$\begin{aligned}
\sigma_{g_1e_1} &= -e^{i\phi}c_1s_1\sigma_{AA} + e^{i\phi}c_1s_1\sigma_{BB} - e^{2i\phi}s_1^2\sigma_{BA} + c_1^2\sigma_{AB},\\
\sigma_{g_2e_2} &= e^{i\phi}c_2s_2\sigma_{CC} - e^{i\phi}c_2s_2\sigma_{DD} - e^{2i\phi}s_2^2\sigma_{DC} + c_2^2\sigma_{CD},\\
\sigma_{g_1e_2} &= e^{i\phi}c_1s_2\sigma_{AC} + e^{i\phi}c_2s_1\sigma_{BD} + e^{2i\phi}s_1s_2\sigma_{BC} + c_1c_2\sigma_{AD},\\
\sigma_{g_2e_1} &= -e^{i\phi}c_2s_1\sigma_{CA} - e^{i\phi}c_1s_2\sigma_{DB} + e^{2i\phi}s_1s_2\sigma_{DA} + c_1c_2\sigma_{CB}.
\end{aligned} \tag{10}$$

The terms on the right of the equal sign correspond to the transitions of different spectral components of Mollow triplets. The first two terms correspond to the Rayleigh line (R), the third term corresponds to the lower sideband, i.e., the fluorescence line (F), and the fourth term corresponds to the higher sideband, i.e., the three-photon line (T). In the frame rotating at the driving laser frequency, the frequencies of the different spectral components of the σ^+ transition can be expressed as

$$\begin{aligned}
\Delta_{\sigma^+,R_1} &= E_C - E_A,\\
\Delta_{\sigma^+,R_2} &= E_D - E_B,\\
\Delta_{\sigma^+,F} &= E_C - E_B,\\
\Delta_{\sigma^+,T} &= E_D - E_A.
\end{aligned} \tag{11}$$

Similarly, the frequencies of the different spectral components of the π transitions can be expressed as

$$\begin{aligned}
\Delta_{\pi,R} &= 0,\\
\Delta_{\pi,F_1} &= E_A - E_B,\\
\Delta_{\pi,F_2} &= E_C - E_D,\\
\Delta_{\pi,T_1} &= E_B - E_A,\\
\Delta_{\pi,T_2} &= E_D - E_C.
\end{aligned} \tag{12}$$

Meanwhile, we define the detunings between the sensors and spectral components of Mollow triplets

$$\begin{aligned}
\delta_{a,l} &= \Delta_a - \Delta_{\sigma^+,l},\\
\delta_{b,l} &= \Delta_b - \Delta_{\pi,l},
\end{aligned} \tag{13}$$

where $\Delta_{\sigma^+,l}$ and $\Delta_{\pi,l}$ are the frequencies of the different spectral components of the σ^+ transition and the π transition defined in Eqs. (11) and (12), respectively, and l denotes the corresponding subscript used in Eqs. (11) and (12).

B. Two-photon transition paths with different time orderings

For the detection scheme of the two-photon correlation we focus on here, two different time orderings of two-photon cascaded emission are involved, that is, a σ^+ photon followed by a π photon [denoted by (σ^+, π)], and the opposite emission ordering [denoted by (π, σ^+)]. In the strong excitation regime, the dressed states are well distinguished, so it is advantageous to consider these emission processes in the dressed-state representation. Therefore, the two-photon cascaded emission with the time ordering (σ^+, π) and (π, σ^+) can be, respectively, decomposed according to Eq. (10) into

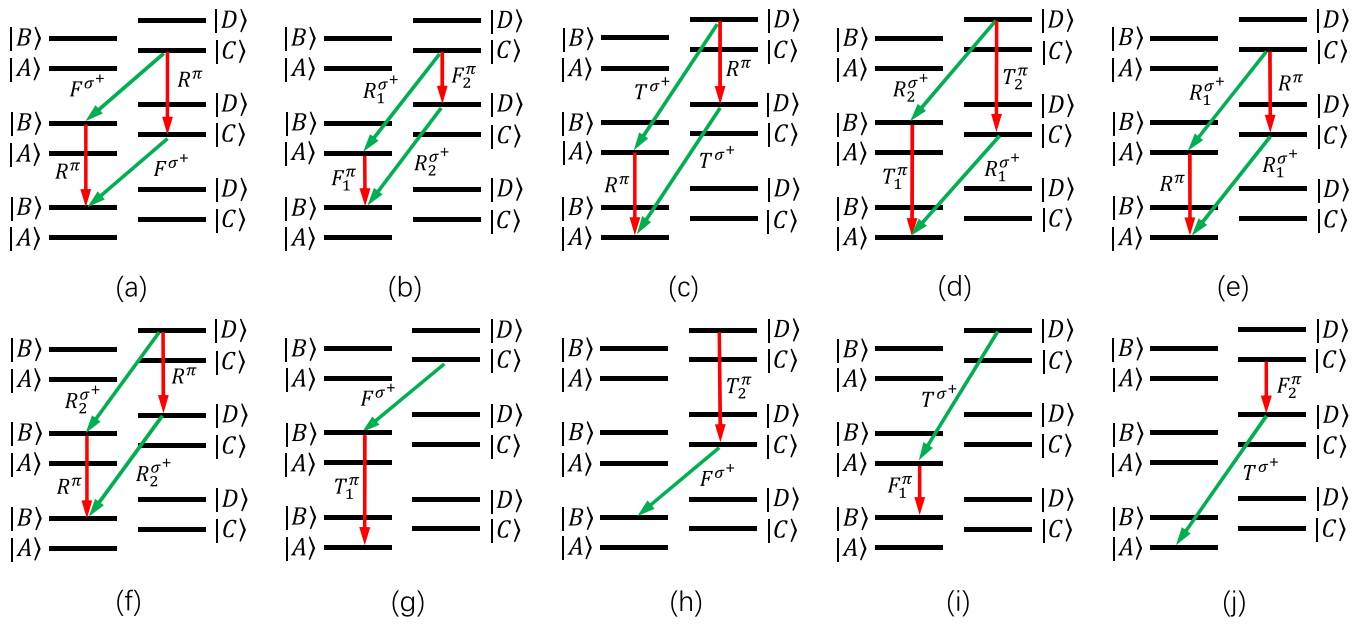

FIG. 3. The dressed-state diagram of the transition paths involved in the two-photon cascade emission of the σ^+ and π transitions. (a)–(j) correspond to different two-photon frequency and interference combinations as shown in Eqs. (14) and (15). It can be seen that σ^+, π photons in (a) are, respectively, from F and R lines labeled by the frequencies (F^{σ^+}, R^{π}); in (b) are, respectively, from R and F lines labeled by the frequencies (R^{σ^+}, F^{π}); in (c) are, respectively, from T and R lines labeled by the frequencies (T^{σ^+}, R^{π}); in (d) are, respectively, from R and T lines labeled by the frequencies (R^{σ^+}, T^{π}); in (e), (f) are both from R lines labeled by the frequencies (R^{σ^+}, R^{π}); in (g), (h) are both from F and T lines labeled by the frequencies (F^{σ^+}, T^{π}); in (i), (j) are both from T and F lines labeled by the frequencies (T^{σ^+}, F^{π}). Obviously, the interference between two-photon transition paths with different time orderings occurs only between two-photon transition paths shown in (a)–(f).

the following forms:

$$\begin{aligned}&(\sigma_{g_1e_1}-\sigma_{g_2e_2})\sigma_{g_1e_2}\\&\quad=\sigma_{g_1e_1}\sigma_{g_1e_2}\\&\quad=\left(-e^{i\phi}c_1s_1\sigma_{AA}-e^{2i\phi}s_1^2\sigma_{BA}\right)\left(e^{i\phi}c_1s_2\sigma_{AC}+c_1c_2\sigma_{AD}\right)\\&\qquad+\left(c_1^2\sigma_{AB}+e^{i\phi}c_1s_1\sigma_{BB}\right)\left(e^{2i\phi}s_1s_2\sigma_{BC}+e^{i\phi}c_2s_1\sigma_{BD}\right),\end{aligned}\tag{14}$$

$$\begin{aligned}&\sigma_{g_1e_2}(\sigma_{g_1e_1}-\sigma_{g_2e_2})\\&\quad=-\sigma_{g_1e_2}\sigma_{g_2e_2}\\&\quad=-\left(e^{i\phi}c_1s_2\sigma_{AC}+e^{2i\phi}s_1s_2\sigma_{BC}\right)\left(e^{i\phi}c_2s_2\sigma_{CC}+c_2^2\sigma_{CD}\right)\\&\qquad-\left(e^{i\phi}c_2s_1\sigma_{BD}+c_1c_2\sigma_{AD}\right)\left(-e^{i\phi}c_2s_2\sigma_{DD}-e^{2i\phi}s_2^2\sigma_{DC}\right).\end{aligned}\tag{15}$$

Here only the transition paths which can physically arise remain and then each of the two-photon emission contains eight possible two-photon transition paths. It can be deduced that the destructive interference between all two-photon paths with different frequencies in Eqs. (14) or (15) result in the total antibunching, i.e., $(\sigma_{g_1e_1}-\sigma_{g_2e_2})\sigma_{g_1e_2}=\sigma_{g_1e_2}(\sigma_{g_1e_1}-\sigma_{g_2e_2})=0$.

In this paper, we mainly focus on the physical processes of two-photon transitions with specific frequency combinations. And, according to the frequency combination of the two photons, the above 16 two-photon transition paths can be divided into ten groups as shown in Fig. 3. If the two-photon transition paths with different time orderings have the same initial and final states, interference between these paths can arise when the time delay between the two successive photon emissions is less than the indeterminacy in the time resolution of detection according to Ref. [48]. This condition can be satisfied in the two-photon paths shown in Figs. 3(a)–3(f), all of which involve photons from the R line. A parallelogram closed loop consisting of two two-photon transition paths with opposite time orderings corresponds to a combination of interference.

It can be seen that each of the four interference combinations Figs. 3(a)–3(d) includes a Rayleigh photon and a sideband photon, which is the same as the case in the Mollow triplet of two-level system [48]. In addition, it should be noted that in the frequency combinations where the two photons are both from R lines, the corresponding interferences between two opposite time orderings can also arise as shown in Figs. 3(e) and 3(f), which does not occur in the interference of time orderings in a conventional two-level system. The reason for the appearance of the interference effect between R lines is that in the level structure we consider, the polarization of two successive transitions are different and then the distinction between two-photon transition paths is not only in the time orderings of frequency but also in the time orderings of polarization.

Remarkably, in terms of the physical origin of the interference of time orderings, there is a significant difference between the case studied here and the conventional interference of time orderings [48,49]. In the latter case, the photons with the same frequencies involved in the two-photon transitions are emitted from the same transition channels, and thus the two two-photon transition paths between which interference of time orderings occurs are both based on the same

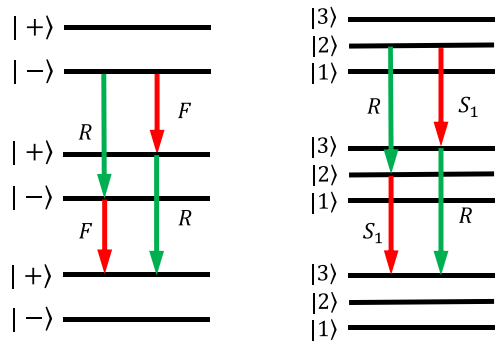

FIG. 4. The dressed-state diagram of the two-photon cascade transitions involved in interference of time orderings. (a) corresponds to the case in the two-level system [48], where the two photons involved are from R and F lines, respectively. (b) corresponds to the case in the Λ-shaped system [49], where the two photons involved are from R and low-frequency inner sideband (labeled by S_1) lines, respectively.

dipole moment or the same combination of dipole moments. For instance, in the interference of time orderings in a two-level system [48] as shown in Fig. 4(a), the two two-photon transition paths with opposite time orderings of emission are composed of a Rayleigh photon and a sideband photon. Both Rayleigh (sideband) photons in these two paths origin from the transition between the excited state and the ground state, thus the interference of time orderings occurs are based on the same dipole moment. In addition, multiple interferences of time orderings are discussed in a Λ-shaped system in Ref. [49]. Similarly to the case in the two-level system, both Rayleigh (sideband) photons involved in the interference between the two-photon transition paths are also emitted from the same transition channels as shown in Fig. 4(b), and then the two two-photon paths involved in the interferences of time orderings are based on the same combination of dipole moments.

However, in the case studied here, it can be seen from Eqs. (14) and (15) that although the two-photon emissions involved in the interferences are both composed of a π photon and a σ^+ photon, the π photons in the two time orderings of emission originate from two different transition channels, i.e., transitions $|e_1\rangle \leftrightarrow |g_1\rangle$ and $|e_2\rangle \leftrightarrow |g_2\rangle$, respectively. Since the dipole moments of these two π transition components are antiparallel, the so-called VICs arise in the corresponding spontaneous emission events, which also explains the physical origin of the unusual interference of time orderings in this paper. In addition, we point out that in the extraordinary biexciton structure of a quantum dot, the interference between different combinations of dipole moments can also be involved [31,50,52]. However, the interference in the biexciton structure originates from the fact that the detector does not distinguish the polarization of emission, which is fundamentally different from the VICs between the two antiparallel dipole moment components of the π transition focused on here. Besides, the which-path information of the two two-photon paths in the biexciton structure depends on the polarizations rather than the time orderings of emission. As the main focus of this paper, next we will discuss this interference of time orderings induced by VICs with the help of analytical expressions in detail.

C. Solution of two-photon correlations

In this section, we focus on the detailed expressions of the frequency-resolved correlations. To write the analytical results compactly, we first define the evolution factors for positive time ordering and negative time ordering of emission as [49]

$$\mathcal{F}^{+}[\omega_o,\omega_e;\omega_\tau,\tau]=\frac{1}{\kappa+2i\omega_e}\left(\frac{1}{\kappa+2i\omega_o}-\frac{e^{-i(\omega_\tau+\frac{\kappa}{2})\tau}}{2\kappa+2i(\omega_o+\omega_e)}\right), \tag{16}$$

$$\mathcal{F}^{-}[\omega_o,\omega_e;\omega_\tau,\tau]=\frac{1}{\kappa+2i\omega_e}\frac{e^{-i(\omega_\tau+\frac{\kappa}{2})\tau}}{2\kappa+2i(\omega_o+\omega_e)}, \tag{17}$$

respectively. The evolution factor for positive emission ordering $\mathcal{F}^{+}[\omega_o,\omega_e;\omega_\tau,\tau]$ describes the situation that the time ordering of two-photon emission is the same as the given detection ordering and increases with the increase of the delay τ. The evolution factor for negative emission ordering $\mathcal{F}^{-}[\omega_o,\omega_e;\omega_\tau,\tau]$ describes the situation that the time ordering of two-photon emission is opposite to the given detection ordering, and decays exponentially to zero with the delay τ with a rate determined by the linewidth (and then the time resolution) of detection. And we point that, for the sake of brevity, the default forms of the evolution factors, i.e., $\mathcal{F}^{\pm}[\omega_o,\omega_e]$, are applied in the case of zero delay in the later sections.

For the cross two-photon correlation between modes a and b mainly discussed in this paper, two different detection orderings of two-photon correlation are involved, that is, the detection of the a photon followed by the detection of the b photon [denoted by (a,b)], and the opposite detection ordering [denoted by (b,a)]. According to the theoretical methods introduced in Appendix B, the analytical expressions of the frequency-resolved two-photon correlations for the detection orderings (a,b) and (b,a) in the limit of short delay are given, respectively, by

$$\mathcal{G}^{(2)}_{ab}(\tau)=\rho_{CC}\left|\mathcal{R}[F^{\sigma^+},R^{\pi};\tau]e^{-iE_B\tau}+\mathcal{R}[R^{\sigma^+},F^{\pi};\tau]e^{-iE_A\tau}\right|^2$$
$$+\rho_{DD}\left|\mathcal{R}[T^{\sigma^+},R^{\pi};\tau]e^{-iE_A\tau}+\mathcal{R}[R^{\sigma^+},T^{\pi};\tau]e^{-iE_B\tau}\right|^2$$

$$+\rho_{CC}\left|\mathcal{R}_1[R^{\sigma^+},R^{\pi};\tau]e^{-iE_A\tau}+\mathcal{R}_1[F^{\sigma^+},T^{\pi};\tau]e^{-iE_B\tau}+\mathcal{R}_2[T^{\sigma^+},F^{\pi};\tau]e^{-iE_A\tau}\right|^2$$
$$+\rho_{DD}\left|\mathcal{R}_2[R^{\sigma^+},R^{\pi};\tau]e^{-iE_B\tau}+\mathcal{R}_2[F^{\sigma^+},T^{\pi};\tau]e^{-iE_B\tau}+\mathcal{R}_1[T^{\sigma^+},F^{\pi};\tau]e^{-iE_A\tau}\right|^2, \quad (18)$$

$$\mathcal{G}^{(2)}_{ba}(\tau)=\rho_{CC}\left|\mathcal{R}[R^{\pi},F^{\sigma^+};\tau]e^{-iE_C\tau}+\mathcal{R}[F^{\pi},R^{\sigma^+};\tau]e^{-iE_D\tau}\right|^2$$
$$+\rho_{DD}\left|\mathcal{R}[R^{\pi},T^{\sigma^+};\tau]e^{-iE_D\tau}+\mathcal{R}[T^{\pi},R^{\sigma^+};\tau]e^{-iE_C\tau}\right|^2$$
$$+\rho_{CC}\left|\mathcal{R}_1[R^{\pi},R^{\sigma^+};\tau]e^{-iE_C\tau}+\mathcal{R}_1[T^{\pi},F^{\sigma^+};\tau]e^{-iE_C\tau}+\mathcal{R}_2[F^{\pi},T^{\sigma^+};\tau]e^{-iE_D\tau}\right|^2$$
$$+\rho_{DD}\left|\mathcal{R}_2[R^{\pi},R^{\sigma^+};\tau]e^{-iE_D\tau}+\mathcal{R}_2[T^{\pi},F^{\sigma^+};\tau]e^{-iE_C\tau}+\mathcal{R}_1[F^{\pi},T^{\sigma^+};\tau]e^{-iE_D\tau}\right|^2, \quad (19)$$

where the subscript in the left of the equal sign represents the specific time ordering of detection, and ρ_{dd} $(d = A, B, C, D)$ represents the steady population of the dressed state $|d\rangle$ of the emitter defined in Eq. (8), whose analytical expression can be obtained in the secular approximation (not shown here). On the right of the equal signs in Eqs. (18) and (19), $\mathcal{R}[L_1, L_2; \tau]$ represents the amplitude of the two-photon emission corresponding to the frequencies (L_1, L_2) shown in Fig. 3 (L_1 and L_2 represent the symbols of the spectral lines applied in Fig. 3), and the ordering of L_1 and L_2 denotes the detection orderings. Therefore, the meanings of the terms in the two-photon correlation $\mathcal{G}^{(2)}_{ab}(\tau)$ in Eq. (18) are given as follows. $\mathcal{R}[F^{\sigma^+}, R^{\pi}; \tau]$ represents the amplitude of the two-photon emission corresponding to the frequencies (F^{σ^+}, R^{π}) shown in Fig. 3(a); $\mathcal{R}[R^{\sigma^+}, F^{\pi}; \tau]$ represents the amplitude of the two-photon emission corresponding to the frequencies (R^{σ^+}, F^{π}) shown in Fig. 3(b); $\mathcal{R}[T^{\sigma^+}, R^{\pi}; \tau]$ represents the amplitude of the two-photon emission corresponding to the frequencies (T^{σ^+}, R^{π}) shown in Fig. 3(c); $\mathcal{R}[R^{\sigma^+}, T^{\pi}; \tau]$ represents the amplitude of the two-photon emission corresponding to the frequencies (R^{σ^+}, T^{π}) shown in Fig. 3(d); $\mathcal{R}_1[R^{\sigma^+}, R^{\pi}; \tau]$ and $\mathcal{R}_2[R^{\sigma^+}, R^{\pi}; \tau]$ represent the amplitudes of the two-photon emissions corresponding to the frequencies (R^{σ^+}, R^{π}) shown in Figs. 3(e) and 3(f), respectively; $\mathcal{R}_1[F^{\sigma^+}, T^{\pi}; \tau]$ and $\mathcal{R}_2[F^{\sigma^+}, T^{\pi}; \tau]$ represent the amplitudes of the two-photon emissions corresponding to the frequencies (F^{σ^+}, T^{π}) shown in Figs. 3(g) and 3(h), respectively; $\mathcal{R}_1[T^{\sigma^+}, F^{\pi}; \tau]$ and $\mathcal{R}_2[T^{\sigma^+}, F^{\pi}; \tau]$ represent the amplitudes of the two-photon emissions corresponding to the frequencies (T^{σ^+}, F^{π}) shown in Figs. 3(i) and 3(j), respectively. For the two-photon correlation $\mathcal{G}^{(2)}_{ba}(\tau)$ in Eq. (19), the two-photon emission amplitudes have one-to-one correspondences with the ones in Eq. (18), and the only difference between them is that the ordering of the detected frequencies in the brackets in Eq. (19) is opposite to the counterparts in Eq. (18), which implies the opposite detection ordering as mentioned earlier. For the sake of compactness, the explicit analytic expressions of the probability amplitudes for the different spectral components of the two-photon transitions are shown in Appendix C. In addition, the explicit analytic expressions of the average populations of sensors a, b are given in Appendix D. Therefore, the normalized frequency-resolved two-photon correlation can be obtained according to Eq. (7).

Naturally, the two-photon correlations in Eqs. (18) and (19) are equal in the case of zero delay, that is, $\mathcal{G}^{(2)}_{ab}(0) = \mathcal{G}^{(2)}_{ba}(0)$, since every two-photon transition amplitude involved is equal to the corresponding term with the opposite detection ordering at $\tau = 0$. Furthermore, we can see from the analytical expressions in Appendix C that the amplitude of each two-photon interference combination contains two terms of the two opposite time orderings, which correspond to the two two-photon transition paths interfering with each other (see Fig. 3). Therefore, the component of the correlation function corresponding to each interference combination can be divided into three parts. The first term is proportional to $|g_{\pi_1}|^2$, which corresponds to the individual contribution of the two-photon transition path with the time ordering (σ^+, π). The second term is proportional to $|g_{\pi_2}|^2$, which corresponds to the individual contribution of the two-photon transition path with the time ordering (π, σ^+). The third term is proportional to $|g_{\pi_1} g_{\pi_2}|$, which corresponds to the contribution of the interference between two two-photon transition paths with opposite time orderings to the two-photon correlation.

As for the detailed physical meaning contained in the third term, on the one hand, since the two two-photon transition paths involved here correspond to two opposite emission orderings, this term reflects the interference effect of time orderings [48,49]. On the other hand, as previously mentioned in Sec. III B, the physical origin of this interference of time orderings is significantly different from that in the conventional studies [48,49]. In the latter case, the two-photon transition paths between which interference of time orderings occurs are based on the same dipole moment [48] or the same combination of dipole moments [49]. However, in the case studied here, we can see from Figs. 3(a)–3(f) that the π photons in the two emission orderings origin from two different transition channels, i.e., transitions $|e_1\rangle \to |g_1\rangle$ and $|e_2\rangle \to |g_2\rangle$, respectively. And, since the dipole moments of these two different π transitions are antiparallel, the effects of VICs between these two transition channels arise in the fluorescence, which induces interference between these different time orderings in the third term. Within the framework of the conventional theory, the effects of VICs can be reflected in the cross term of nonorthogonal transmit field operators [12] or filtered field operators. However, in this paper, the filtering and detection of the fluorescence are also considered in the system as the subjects of the theoretical study, such that the effects of VICs are formally represented as the term proportional to $|g_{\pi_1} g_{\pi_2}|$ in Eqs. (18) and (19). From the view of understanding, if the form of the frequency-resolved correlation function in the sensor method in Eq. (7) was restored to the one in the conventional theory [21], this correspondence would be more clearly manifested. We can see that in the absence of VICs, the above-mentioned interference of time orderings would not

appear. Thus, this interference can be viewed as a demonstration of VICs. In the following sections, we will discuss the interference of time orderings induced by VICs in detail according to specific situations.

IV. INTERFERENCE OF TIME ORDERINGS

In this section, we mainly focus on the theoretical discussion of the effects of VICs that arise in the frequency-resolved two-photon correlations between the spectral components of the fluorescence triplets from σ^+ and π transitions, respectively. Before this, we recall that the effects of VICs can also arise in the two-photon correlations of π transitions as mentioned in Ref. [12]. However, for the establishment of this interference effect, the spontaneous emission from the σ transition was needed as the bridge between the two different π transitions. Therefore, the contribution of VICs to the correlation can be significant only when the delay between two successive transitions is at a timescale of the order of γ_3 (or γ_4). In this paper, we choose the cross correlation of σ^+ and π transitions as the research object. We analyze the properties of the correlations between different spectral components, and find that the effects of VICs can also arise in the frequency-resolved correlations (even at a timescale much smaller than the lifetime of the level system).

A. Degenerate system

First, we consider the case of the degenerate system ($B_L = \delta = 0$), where the frequencies of the two π transitions are equal, and two effective Rabi frequencies of dressed states are also equal, i.e., $\bar{\Omega}_1 = \bar{\Omega}_2$, so the two two-level folds in Fig. 2 are symmetrical. In the strong excitation regime, the different dressed states can be well distinguished and the frequencies of the emissions are concentrated near the lines of the Mollow triplet. We note that the following discussion will mainly focus on this case.

In Fig. 5, we show the two-photon correlation function at zero delay (i.e., $\tau = 0$) as a function of the setting frequency of the sensor (or the filter). Figures 5(a)–5(c) correspond to the cases where sensor b is tuned to the F line, R line and T line, respectively, and then contain the information of the correlation functions of all the frequency combinations shown in Fig. 3. It can be seen that the analytical expressions Eqs. (18) and (19) of the two-photon correlation functions are in good agreement with the exact numerical results.

To explore the detailed information of spectral components contained in correlations, we focus on a specific situation where the sensors are tuned near the frequencies (R^{σ^+}, F^{π}). Therefore, in the strong excitation regime, only the two transition paths shown in Fig. 3(b) really need to be considered. And for the degeneracy of the system, we can define $\delta_{a,R} = \delta_{a,R_1} = \delta_{a,R_2}$ and $\delta_{b,F} = \delta_{b,F_1} = \delta_{b,F_2}$ [the definitions of δ_{a,R_i} and δ_{b,F_i} are given in Eq. (13)]. Therefore, within the rotating wave approximation, the analytical expressions Eqs. (18) and (19) of the frequency-resolved two-photon correlations for the detection orderings (a, b) and (b, a) in the limit of short

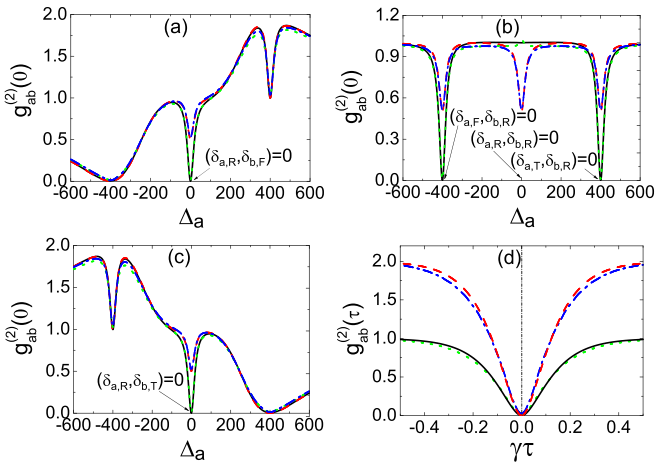

FIG. 5. For the degenerate system ($B_L = \delta = 0$), the frequency-resolved two-photon correlation at zero delay is plotted as a function of the detunning Δ_a scaled by γ for $\Delta_b = -\bar{\Omega}_1$ in (a), $\Delta_b = 0$ in (b), and $\Delta_b = \bar{\Omega}_1$ in (c). Therefore, all two-photon interference combinations shown in Figs. 3(a)–3(f) are included in (a)–(c). In addition, at the detected frequencies (R^{σ^+}, F^{π}), the frequency-resolved correlation is plotted as a function of the delay τ for $\delta_{a,R} = \delta_{b,F} = 0$ in (d). Other parameters are $\Omega = 200\gamma$, $\kappa_a = \kappa_b = 20\gamma$, and $\Delta = 0$. The black solid line and the green dotted line, respectively, represent the analytical and numerical results of the two-photon correlation in the presence of VICs; the red dashed line and the blue dash-dotted line, respectively, represent the analytical and numerical results of the two-photon correlation in the absence of VICs.

delay reduce, respectively, to

$$\begin{aligned}\mathcal{G}^{(2)}_{ab}(\tau) =& \rho_{CC}|\mathcal{R}[R^{\sigma^+}, F^{\pi}; \tau]|^2 \\ =& \rho_{CC}|4g_{\sigma}s_1s_2(g_{\pi_1}c_1s_1\mathcal{F}^{+}[\delta_{a,R}, \delta_{b,F}; \delta_{b,F}, \tau] \\ &+ g_{\pi_2}c_2s_2\mathcal{F}^{-}[\delta_{a,R}, \delta_{b,F}; \delta_{b,F}, \tau])|^2, \end{aligned} \tag{20}$$

$$\begin{aligned}\mathcal{G}^{(2)}_{ba}(\tau) =& \rho_{CC}|\mathcal{R}[F^{\pi}, R^{\sigma^+}; \tau]|^2 \\ =& \rho_{CC}|4g_{\sigma}s_1s_2(g_{\pi_1}c_1s_1\mathcal{F}^{-}[\delta_{b,F}, \delta_{a,R}; \delta_{a,R}, \tau] \\ &+ g_{\pi_2}c_2s_2\mathcal{F}^{+}[\delta_{b,F}, \delta_{a,R}; \delta_{a,R}, \tau])|^2. \end{aligned} \tag{21}$$

It can be seen that the correlation for each detection ordering includes the contributions of the two-photon transition paths with the two emission orderings (σ^+, π) and (π, σ^+). Under the parameter condition focused on in this paper, these two-photon transition paths both start from the same initial state where the emitter is in the dressed state $|C\rangle$ and the sensors a, b are both in the vacuum states as shown in Fig. 3(b), which results in the common factor ρ_{CC} in Eqs. (20) and (21). The contributions of the path with the time ordering (σ^+, π) in the case of two detection orderings, respectively, correspond to the evolution factors $\mathcal{F}^{+}[\delta_{a,R}, \delta_{b,F}; \delta_{b,F}, \tau]$ and $\mathcal{F}^{-}[\delta_{b,F}, \delta_{a,R}; \delta_{a,R}, \tau]$; the contributions of the path with the time ordering $(\pi; \sigma^+)$ in the case of two detection orderings, respectively, correspond to the evolution factors $\mathcal{F}^{-}[\delta_{a,R}, \delta_{b,F}; \delta_{b,F}, \tau]$ and $\mathcal{F}^{+}[\delta_{b,F}, \delta_{a,R}; \delta_{a,R}, \tau]$. And, the cross terms of the two opposite emission orderings in Eqs. (20) and (21) correspond to the interference of time orderings. As discussed in Sec. III,

different from the case in the conventional interference of time orderings [48,49], the two two-photon paths involved here are based on different combinations of dipole moments as shown in Fig. 3(b), between which the interference is induced by VICs arising between the two antiparallel components of the π transitions.

First, we focus on the two-photon correlations in the case of zero delay ($\tau = 0$), therefore, Eqs. (20) and (21) are equivalent as mentioned in Sec. III C. We can see from Eq. (20) [or (21)] that at the one-photon resonance $\delta_{a,R} = \delta_{b,F} = 0$, the values of the two-photon transition amplitudes of the two opposite emission orderings are equal, that is, $\mathcal{F}^{+}[\delta_{a,R}, \delta_{b,F}] = \mathcal{F}^{-}[\delta_{a,R}, \delta_{b,F}]$. However, since the dipole moments of the two π transitions are antiparallel, the coupling coefficients of sensor b with π transitions satisfies $g_{\pi_1} = -g_{\pi_2}$. Therefore, complete destructive interference appears between two two-photon transition paths with different time orderings, which results in that the normalized two-photon correlation is equal to zero and a perfect antibunching arises. Obviously, this effect is different from the antibunching which is caused by the nonemitting of the final state in the frequency-blind correlation, and origins from the finite time resolution of detection. Similarly, it can be found that the perfect antibunching caused by the destructive interference can occur at the detected frequencies (F^{σ^+}, R^{π}), (T^{σ^+}, R^{π}), and (R^{σ^+}, T^{π}) when the corresponding resonance conditions are satisfied as labeled in Figs. 5(b) and 5(c). In addition, at the detected frequencies (R^{σ^+}, R^{π}), the interference effect can also arise, which exhibits as perfect uncorrelation at resonance as labeled in Fig. 5(b).

It should be noted that the antibunching caused by the destructive interference between two-photon transition paths with different time orderings is also reported in Refs. [48,49], where the two-photon paths involved origin from the same dipole moment combination. However, for the system studied in this paper, it can be seen from Eq. (20) that the π photons in the transition paths with different time orderings origin from two different dipole moment combinations. And due to the VICs between different dipole moments, interference between different emission orderings can occur.

If the interference between different emission orderings induced by VICs is ignored, the corresponding two-photon correlations will be significantly different. To demonstrate this difference, we show the two-photon correlation that does not consider the effects of VICs (as shown by the blue dash-dotted line), that is, assuming that the term proportional to $|g_{\pi_1} g_{\pi_2}|$ in Eq. (20) is equal to zero. In this case, we see that obvious dips still appear due to the resonance effect, but the perfect antibunching disappears since there is no destructive interference. Compared to the perfect antibunching in the presence of VICs, the value of the normalized two-photon correlation at resonance is raised to about $1/2$ in the absence of VICs. Therefore, there is no doubt that these dips that reach zero in the spectrum of the two-photon correlation are the clear signatures of VICs. Moreover, unlike the work in Ref. [12] where the effects of VICs on the two-photon correlation can only be apparent at a timescale of the order of γ_{σ}^{-1}, the effects of VICs can obviously arise at zero delay in this work.

Next, we consider the frequency-resolved two-photon correlations in the case of a given time ordering of detection, that is, $\tau \neq 0$. For the degenerate system ($B_L = \delta = 0$) discussed in this section, it is easy to see that the contributions of the two emission orderings to the two-photon correlations in Eqs. (20) and (21) have a good time antisymmetry in the two opposite detection orderings as shown in Fig. 5(d). In addition, the correlation function in the absence of VICs is also shown as a contrast, which allows the effects of VICs to be visualized as a function of the delay τ between two successive detections. We can see that when the delay is much smaller than the indeterminacy in the time resolution of detection, i.e., $\tau \ll \kappa^{-1}$, the two-photon correlation is close to the case at zero delay, and then VICs and its resulting antibunchling are maintained well. When the delay τ increases and exceeds this indeterminacy, the VIC effects decrease and vanish rapidly. This change of the VIC effects with the delay τ can be well explained by the analogy with the conventional interference effect of different time orderings. We can see from Eqs. (20) and (21) that in two time orderings of detection, the two-photon correlations both contain the contributions of the positive and negative emission orderings.

For certain time orderings of detection, the contributions of the two opposite emission orderings become unequal. This unequality becomes obvious with the increase of delay τ, and then the effects of VICs become weak. When the delay τ is much larger than the indeterminacy in the time resolution of detection, i.e., $\tau \gg \kappa^{-1}$, the contribution of the negative emission orderings tends to zero according to Eq. (17). In this case, the time orderings of detection are just the time orderings of emission, and the interference effects between different time orderings of emission, that is, the effects of VICs, disappear. Therefore, we can conclude that to observe the interference of time orderings induced by VICs described here, it must be ensured that the delay τ between two successive detections is shorter than the indeterminacy in the time resolution of detection.

B. Nondegenerate system

The interference of time orderings studied here arises between two-photon paths based on different combinations of dipole moments, which means that the manipulation of the corresponding interference effects may be realized easily. Following this idea, in this section, we discuss the two-photon correlations in the case of a nondegenerate system, that is, the case where an external magnetic field is applied to the emitter. From the Hamiltonian of the quantum emitter in Eq. (1), it can be seen that the effect of the external magnetic field is reflected in the parameters B_L and δ. By analyzing the level structure in the dressed-state representation, we see that the effect of the parameter B_L is only reflected as a trivial frequency shift of the fold composed of the states C, D as shown in Eq. (9). However, the parameter δ can change the effective Rabi frequencies in the dressed-state representation according to the definitions in Sec. III A. Therefore, as for the π transitions, a frequency difference occurs between the same sideband lines which are, respectively, from transitions $|e_1\rangle \to |g_1\rangle$ and $|e_2\rangle \to |g_2\rangle$, that is, $\Delta_d = \Delta_{\pi,T_2} - \Delta_{\pi,T_1} = \Delta_{\pi,F_1} - \Delta_{\pi,F_2} = \bar{\Omega}_2 - \bar{\Omega}_1$ according to Eqs. (11) and (12), while the frequencies of the R lines are not affected.

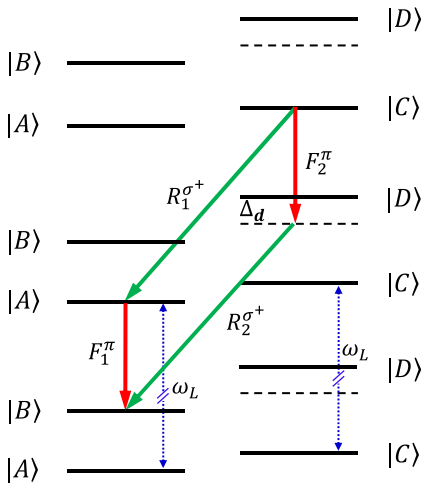

FIG. 6. The dressed-state diagram of the two-photon cascaded transitions corresponding to the detected frequencies (R^{σ^+}, F^π) in the case of nondegenerate system. Two two-photon transition paths with opposite time orderings are involved. The external magnetic field can cause a detuning Δ_d, which have a significant effect on the interference between these two opposite time orderings.

Based on the above rules, we consider the effect of the external magnetic field on the two-photon transitions discussed in Sec. III. We can see that of all interference combinations of two-photon transition paths with different time orderings shown in Fig. 3, only the combinations where the π photon is from sidebands, that is, the detected frequencies (R^{σ^+}, F^π) and (R^{σ^+}, T^π), include the effect of the detuning δ caused by the external magnetic field. A significant consequence of the effect of the external magnetic field on the emitter is that two two-photon paths with opposite time orderings, which could not be distinguished in frequencies in the case of the degenerate system, become distinguishable by the sensor (or the detector). Therefore, it can be expected that the interference effects in the frequency-resolved two-photon correlations can be significantly changed and we will explore this change in detail according to the analytical results obtained in Sec. III C.

1. Effect of external magnetic field

As we have mentioned above, the effect of the detuning δ caused by the external magnetic field can only be reflected at the detected frequencies (R^{σ^+}, F^π) and (R^{σ^+}, T^π). To further understand the effect of the external magnetic field and considering the similarity of these two interference combinations, we also choose the detected frequencies (R^{σ^+}, F^π) as the main research object to discuss the two-photon correlations of the nondegenerate system in detail, and the corresponding diagram of the two-photon cascaded transitions is shown Fig. 6. Therefore, within the rotating wave approximation, the analytical expressions Eqs. (18) and (19) of the frequency-resolved two-photon correlations for the detection orderings (a, b) and (b, a) in the limit of short delay reduce, respectively, to

$$\begin{aligned}\mathcal{G}_{ab}^{(2)}(\tau) =& \rho_{CC}|\mathcal{R}[R^{\sigma^+}, F^\pi; \tau]|^2 \\ =& \rho_{CC}\big|4g_\sigma s_1 s_2\big(g_{\pi_1} c_1 s_1 \mathcal{F}^+\big[\delta_{a,R_1}, \delta_{b,F_1}; \delta_{b,F_1}, \tau\big] \\ &+ g_{\pi_2} c_2 s_2 \mathcal{F}^-\big[\delta_{a,R_2}, \delta_{b,F_2}; \delta_{b,F_1}, \tau\big]\big)\big|^2, \end{aligned} \tag{22}$$

$$\begin{aligned}\mathcal{G}_{ba}^{(2)}(\tau) =& \rho_{CC}|\mathcal{R}[F^\pi, R^{\sigma^+}; \tau]|^2 \\ =& \rho_{CC}\big|4g_\sigma s_1 s_2\big(g_{\pi_1} c_1 s_1 \mathcal{F}^-\big[\delta_{b,F_1}, \delta_{a,R_1}; \delta_{a,R_2}, \tau\big] \\ &+ g_{\pi_2} c_2 s_2 \mathcal{F}^+\big[\delta_{b,F_2}, \delta_{a,R_2}; \delta_{a,R_2}, \tau\big]\big)\big|^2. \end{aligned} \tag{23}$$

Similar to the case of the degenerate system in Sec. IV A, the correlation for each time ordering of detection also includes the contributions of the two emission orderings (σ^+, π) and (π, σ^+). The contributions of the path with the time ordering (σ^+, π) in the case of two detection orderings correspond to the evolution factors $\mathcal{F}^+[\delta_{a,R_1}, \delta_{b,F_1}; \delta_{b,F_1}, \tau]$ and $\mathcal{F}^-[\delta_{b,F_1}, \delta_{a,R_1}; \delta_{a,R_2}, \tau]$, respectively; the contributions of the path with the time ordering (π, σ^+) in the case of two detection orderings correspond to the evolution factors $\mathcal{F}^-[\delta_{a,R_2}, \delta_{b,F_2}; \delta_{b,F_1}, \tau]$ and $\mathcal{F}^+[\delta_{b,F_2}, \delta_{a,R_2}; \delta_{a,R_2}, \tau]$, respectively. And, the cross terms of the two opposite emission orderings in Eqs. (22) and (23) correspond to the interference of time orderings induced by VICs. Different from the case of the degenerate system in Eqs. (20) and (21), we see that the frequencies in the two two-photon paths involved in the same time orderings of detection are different, which means that the manipulation of the interference effects of time orderings may be realized by adjusting these frequencies. And, according to the definitions in Sec. III A, we can see that when the parameter δ is adjusted, the total frequencies of these two coherent two-photon transitions remain equal, i.e., $\delta_{a,R_1} + \delta_{b,F_1} = \delta_{a,R_2} + \delta_{b,F_2}$. However, the frequency differences between the one-photon transitions coupled to the same sensors in these two paths can occur and satisfy $\Delta_d = \delta_{a,R_2} - \delta_{a,R_1} = \delta_{b,F_1} - \delta_{b,F_2}$. Then, if one of the two two-photon paths is kept resonant with the two sensors when adjusting the parameter δ, the other path must be nonresonant and the detunings are Δ_d.

More specifically, we focus on the two-photon correlations in the case of zero delay ($\tau = 0$). We assume that when the effective Rabi frequencies of the dressed states and then the frequencies of the different triplet components are changed by the magnetic field, the sensors are always kept resonant with the two-photon transition path with the emission ordering (σ^+, π), i.e., $\delta_{a,R_1} = \delta_{b,F_1} = 0$. Then, the evolution factors for this emission ordering, i.e., $\mathcal{F}^+[\delta_{a,R_1}, \delta_{b,F_1}]$ and $\mathcal{F}^-[\delta_{b,F_1}, \delta_{a,R_1}]$, always remain a maximum. In contrast, the frequency difference induced by the parameter δ causes the evolution factors for the opposite time ordering of emission, i.e., $\mathcal{F}^-[\delta_{a,R_2}, \delta_{b,F_2}]$ and $\mathcal{F}^-[\delta_{b,F_2}, \delta_{a,R_2}]$, to decrease due to nonresonance. Therefore, compared to the case of the degenerate system, the interference of time orderings induced by VICs and then the perfect antibunching caused by the destructive interference are weakened.

To visually show the effect of adjusting the magnetic field on the frequency-resolved two-photon correlation, we plot the correlation as the function of the parameter δ in Fig. 7(a), and the individual contributions of the two emission orderings to the two-photon correlation are exhibited simultaneously. We set the detection linewidths $\kappa = 6\gamma$, and it can be seen that when the parameter δ reaches about 25γ, the one-photon detuning Δ_d of the above nonresonant two-photon path is close to the indeterminacy in the time resolution of detection. In this case, the which-path information of the two-photon transitions can be well distinguished by the detectors. Therefore, we see

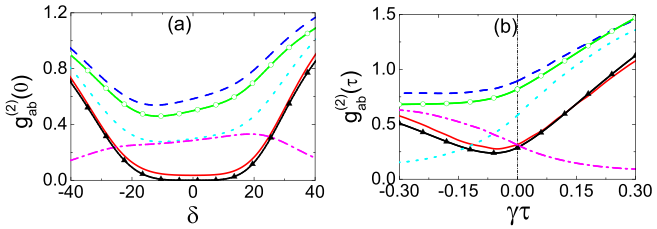

FIG. 7. The two-photon correlation at the detected frequencies (R^{σ^+}, F^{π}) is plotted as a function of the detuning δ scaled by γ induced by the external magnetic field in (a), and as a function of the delay τ for $\delta = 25\gamma$ in (b). The sensors are kept resonant with the two-photon transition path with the emission ordering (σ^+, π), and other parameters are $\Omega = 50\gamma$, $\kappa_a = \kappa_b = 6\gamma$, and $\Delta = 0$. The black triangular line and the red solid line, respectively, represent the analytical and numerical results of the two-photon correlation in the presence of VICs; the green circular line and the blue dashed line, respectively, represent the analytical and numerical results of the two-photon correlation in the absence of VICs; the cyan dotted line and the magenta dash-dotted, line respectively, represent the individual contributions of two two-photon transition paths with the emission orderings (σ^+, π) and (π, σ^+).

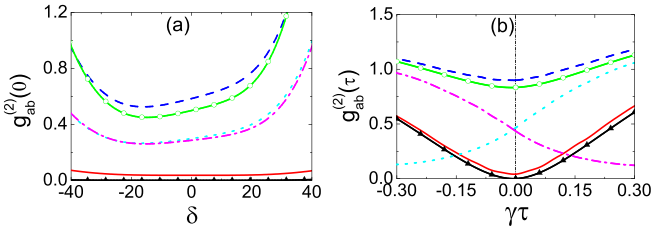

FIG. 8. The two-photon correlation at the detected frequencies (R^{σ^+}, F^{π}) is plotted as a function of the detuning δ scaled by γ induced by the external magnetic field in (a), and as a function of the delay τ for $\delta = 25\gamma$ in (b). The filtering frequencies of the two sensors are respectively tuned to the middle frequencies of two sets of one-photon transitions coupled to them, that is, $\delta_{a,R_1} = -\delta_{b,F_1} = -\delta_{a,R_2} = \delta_{b,F_2} = \frac{\Delta_d}{2}$, and other parameters are the same as in Fig. 7. The black triangular line and the red solid line, respectively, represent the analytical and numerical results of the two-photon correlation in the presence of VICs; the green circular line and the blue dashed line, respectively, represent the analytical and numerical results of the two-photon correlation in the absence of VICs; the cyan dotted line and the magenta dash-dotted line, respectively, represent the individual contributions of the two two-photon transition paths with the emission orderings (σ^+, π) and (π, σ^+).

that the individual contributions of the two emission orderings become unequal obviously, so the interference of time orderings induced by VICs and the resulting antibunching reduce significantly and two-photon correlations in the presence and absence of VICs are close. As the parameter δ increase, the amplitude of the nonresonant two-photon path disappears gradually, therefore the two-photon correlation approaches the case of single transition path without any interference and the effects of VICs fade away.

Next, we consider the two-photon correlations in the case of $\tau \neq 0$ maintaining the above setting frequencies of the sensors. When $\tau > 0$, the time ordering of detection is (a, b) and the emission ordering of the resonant two-photon path is the same as this detection ordering, so the corresponding evolution factor $\mathcal{F}^+[\delta_{a,R_1}, \delta_{b,F_1}; \delta_{b,F_1}, \tau]$ increases with the increase of the delay τ according to Eq. (16). However, the evolution factor for the opposite emission ordering $\mathcal{F}^-[\delta_{a,R_2}, \delta_{b,F_2}; \delta_{b,F_1}, \tau]$ reduces due to nonresonance. Therefore, the destructive interference effect between two-photon transition paths with different time orderings is suppressed. In this case, we see from Fig. 7(b) that, compared to the case of the degenerate system in Fig. 5(d), the distinction between two-photon correlations in the presence and absence of VICs is greatly reduced, and the overall two-photon correlation becomes much stronger.

When $\tau < 0$, the time ordering of detection is (b, a) and the emission ordering of the resonant two-photon path is opposite to this detection ordering, so the corresponding evolution factor $\mathcal{F}^-[\delta_{b,F_1}, \delta_{a,R_1}; \delta_{a,R_2}, \tau]$ reduces with the increase of the delay τ according to Eq. (17). Meanwhile, the evolution factor for the positive emission time ordering $\mathcal{F}^+[\delta_{b,F_2}, \delta_{a,R_2}; \delta_{a,R_2}, \tau]$ also reduces due to nonresonance. In this case, the corresponding two-photon correlation is significantly weaker than one in the case of the degenerate system discussed in Sec. IV A, and thus is obviously different from one in the case when $\tau > 0$ as shown in Fig. 7(b).

Therefore, we can conclude that in the above system with one-photon frequency differences between the two-photon paths with different time orderings, the evolution of the two-photon correlation function with delay τ can exhibits obvious asymmetry since the two-photon path with a specific time ordering is selected in the detection. A similar time asymmetry can also arise when the sensors are kept resonant with the two-photon transition path with the time ordering (π, σ^+) (not shown here). Moreover, according to the analytical expression obtained in Sec. III C., it can be expected that the laws found above are also valid for the detected frequencies (R^{σ^+}, T^{π}).

2. Manipulation by frequency filtering

In the above section, we point out that for certain two-photon frequency combinations, the detuning δ induced by the external magnetic field can break the degeneracy of the one-photon frequencies in the two-photon transition paths with different time orderings, so which-path information of the two-photon transitions can be revealed and the interference of time orderings and time symmetry are destroyed. On the other hand, some recent studies [28,31,50–52] based on the biexciton structure in a quantum dot show that by adjusting the filtering frequency externally, the erasure of the which-path information revealed by the fine-structure splitting can be realized, and then the entanglement of the quantum source is restored to the state where the effect of splitting is eliminated. Inspired by these schemes and considering the similarity between the biexciton structure in a quantum dot and the level structure discussed in this paper, we next research the effects of adjusting the filtering frequency on the frequency-resolved two-photon correlations.

Similarly, we first focus on the two-photon correlation in the case of zero delay. We see from Fig. 8(a) that when the filtering frequencies of the two sensors are, respectively, tuned to the middle frequencies of two sets of one-photon transitions

coupled to them, that is, $\delta_{a,R_1} = -\delta_{b,F_1} = -\delta_{a,R_2} = \delta_{b,F_2} = \frac{\Delta_d}{2}$, the broken antibunching effect mentioned in the previous section restores. We can explain the physical origin of this phenomenon by means of the analytical expression Eqs. (22) or (23) for the two-photon correlations. When the filtering frequencies are, respectively, set as mentioned above, the spectral components containing the which-path information of the two-photon transitions can be filtered out, so the two-photon transition paths of the two different time orderings become indistinguishable by the detectors. According to the analytical expression Eq. (22), we can derive that the amplitudes of the two-photon transition paths with different time orderings almost return to equal value (as shown by the cyan dotted line and the magenta dash-dotted line), and then the complete destructive interference and resulting perfect antibunching effect recover. We see that the contribution of each two-photon path is nonzero and increases with the increase of Δ_d due to δ, and then the corresponding two-photon correlation in the absence of VICs increases rapidly as shown by the blue dashed line in Fig. 8(a). However, when the interference of time orderings induced by VICs is included, the two-photon correlation is always maintained at near zero. Therefore, the distinction between the two-photon correlations in the presence and absence of VICs becomes more and more obvious as the value of δ increases, which greatly facilitates the observation of the effects of VICs.

For the case of $\tau \neq 0$, maintaining the above filtering frequencies and other parameters, it can be seen from Fig. 8(b) that the time symmetry of the correlation restores. For the two-photon transition paths of the two different time orderings involved in the detected frequencies selected, the evolution of the corresponding correlations with the delay depends entirely on the evolution factors, that is, $\mathcal{F}^+[\delta_{a,R_1}, \delta_{b,F_1}; \delta_{b,F_1}, \tau]$ and $\mathcal{F}^-[\delta_{b,F_1}, \delta_{a,R_1}; \delta_{a,R_2}, \tau]$ corresponding to the emission ordering (σ^+, π), and $\mathcal{F}^-[\delta_{a,R_2}, \delta_{b,F_2}; \delta_{b,F_1}, \tau]$ and $\mathcal{F}^+[\delta_{b,F_2}, \delta_{a,R_2}; \delta_{a,R_2}, \tau]$ corresponding to the emission ordering (π, σ^+). It can be seen from Eqs. (22) and (23) that when tuning the filtering frequency of each sensor to the middle frequency of the one-photon transitions coupled to them, the contributions of the two emission orderings to the two-photon correlations restore the time antisymmetry in the two opposite detection orderings (as shown by the cyan dotted line and the magenta dash-dotted line) similar to the case of the degenerate system, and then the time symmetry of the quantum correlation recovers again. This shows the erasure of the information of time orderings by the manipulation of frequency filtering.

V. CONCLUSION

The frequency-resolved correlations of the π and σ^+ transitions are theoretically investigated in the $J = 1/2$ to $J = 1/2$ system in the large detection linewidth and strong excitation regime. The quantum emitter and detectors are both treated as the quantized objects and entirely included in a combined system, which is more consistent with the consideration of quantum mechanics. By studying the frequency-resolved correlations in the case of degenerate system, it has been shown that the interference effects of time orderings between different dipole moments can appear due to the effects of VICs, which can exhibit as perfect antibunching or uncorrelation, depending on the selected combination of the spectral lines in the fluorescence triplets. Therefore, the cross frequency-resolved correlation of the π and σ^+ transitions can serve as a good scheme to observe the effects of VICs. Meanwhile, the interference effects of time orderings become weak with the increase of delay of the two-photon correlations. When the delay is much larger than the indeterminacy in the time resolution of detection, the effects of VICs, that is, the interference of time orderings, disappear.

In addition, we have found that in the two-photon transitions consisting of a π photon from the T or F line and a σ^+ photon from the R line, the external magnetic field can cause the frequency differences between the one-photon transitions with the same polarizations. Choosing the two-photon transitions consisting of a π photon from the T line and a σ^+ photon from the R line as the research object, we have discussed the effect of the external magnetic field on the frequency-resolved two-photon correlation. It has been shown that when the single-photon frequency differences caused by the external magnetic field can be distinguished by the detectors, the 'which path' information of the two-photon transitions is revealed, which causes that the interference of time orderings induced by VICs and time symmetry of the two-photon correlations are destroyed. However, by tuning the filtering frequencies to the middle frequencies of the one-photon transitions coupled to them, the which-path information can be erased, so the perfect interference effects of time orderings are recovered. Therefore, the system studied in this paper can be a candidate to demonstrate quantum erasure.

ACKNOWLEDGMENTS

This work is supported by the National Natural Science Foundation of China (Grants No. 11774118 and No. 11474119) and the Fundamental Research Funds for the Central Universities of MOE (Grants No. CCNU18CXTD01 and No. CCNU17TS0006).

APPENDIX A: CALCULATION OF SYSTEM PARAMETERS

Within the rotating wave approximation, the interaction Hamiltonian of the quantum emitter with the driving laser filed takes the form

$$H_I = V_{e_1g_1}\sigma_{e_1g_1}e^{-i\omega_L t} + V_{e_2g_2}\sigma_{e_2g_2}e^{-i\omega_L t} + \text{H.c.} \tag{A1}$$

According to the Wigner-Eckart theorem [53,54], the interaction coefficient can be explicitly given by

$$\begin{aligned} V_{e_ig_i} &= -\langle J_e, m_{e_i}|\mathbf{d}|J_g, m_{g_j}\rangle \cdot \mathbf{E} \\ &= (-1)^{J_e - m_{e_i}+1}\begin{pmatrix} J_e & 1 & J_g \\ -m_{e_i} & q & m_{g_i}\end{pmatrix}\Omega_L, \end{aligned} \tag{A2}$$

where $\mathbf{d}$ is the electric dipole operator, J_e and J_g are, respectively, the total angular momentum quantum numbers of the ground and excited states, $\mathbf{E}$ is the electric-field vector, $\Omega_L = \langle J_e \parallel \mathbf{d} \parallel J_g\rangle E$ is the Rabi frequency of the light field, and $q = 0$ for the π-polarized driving laser applied in this paper. The 2×3 matrices in parentheses are the Wigner 3j symbols, whose calculation can be conveniently performed by the built-in function of MATHEMATICA. Substituting the

specific parameters into Eq. (A2), we can obtain the interaction coefficients as $V_{e_1g_1} = \Omega_L/\sqrt{6}$ and $V_{e_2g_2} = -\Omega_L/\sqrt{6}$.

In addition, according to Ref. [55], the spontaneous decay rate is given by

$$\gamma_{m_g,m_g'}^{m_e,m_e'} = (-1)^{2J_g-m_g-m_g'}(2J_e+1)\gamma \sum_{q=-1}^{1} \begin{pmatrix} J_g & 1 & J_e \\ -m_g & q & m_e \end{pmatrix} \begin{pmatrix} J_g & 1 & J_e \\ -m_g' & q & m_e' \end{pmatrix}, \tag{A3}$$

where γ represents the total spontaneous decay rate of the transition $J = 1/2$ to $J = 1/2$. Then we can obtain $\gamma_1 = \gamma_{-\frac{1}{2},-\frac{1}{2}}^{-\frac{1}{2},-\frac{1}{2}} = \gamma/3$, $\gamma_2 = \gamma_{\frac{1}{2},\frac{1}{2}}^{\frac{1}{2},\frac{1}{2}} = \gamma/3$, $\gamma_{12} = \gamma_{-\frac{1}{2},\frac{1}{2}}^{-\frac{1}{2},\frac{1}{2}} = -\gamma/3$, $\gamma_{21} = \gamma_{\frac{1}{2},-\frac{1}{2}}^{\frac{1}{2},-\frac{1}{2}} = -\gamma/3$, $\gamma_3 = \gamma_{\frac{1}{2},\frac{1}{2}}^{-\frac{1}{2},-\frac{1}{2}} = 2\gamma/3$, and $\gamma_4 = \gamma_{-\frac{1}{2},-\frac{1}{2}}^{\frac{1}{2},\frac{1}{2}} = 2\gamma/3$.

APPENDIX B: ANALYTICAL METHOD FOR SOLVING CORRELATION FUNCTIONS

In this Appendix, we present the specific method used to solve the frequency-resolved two-photon correlation function analytically. For the calculation of the cross second-order correlation, two sensors are needed to be included in the system according to the sensor method [22]. In the limit of the vanishing coupling between the sensors and quantum emitter, each sensor can be considered as a two-level system composed of the ground state $|0_s\rangle$ and the excited state $|1_s\rangle$ $(s = a, b)$. Therefore, the quantum state in the Hilbert space composed of the emitter and sensors can be expressed as $|m, n_a, n_b\rangle$, where $m = A, B, C, D$ represents the dressed state of the emitter and $n_s = 0, 1$ represents the excitation number of sensor s.

Considering a measurement where the detection of sensor b takes place after a delay τ with respect to the detection of sensor a which takes place in the steady-state limit of the system. We choose the time when the detection of sensor a takes place as the starting point of time, therefore the two-photon correlation function can be expressed as

$$\begin{aligned} \mathcal{G}_{ab}^{(2)}(\tau) &= \mathrm{Tr}[a^\dagger(0)b^\dagger(\tau)b(\tau)a(0)\rho_{\mathrm{st}}] \\ &= \mathrm{Tr}[b^\dagger b\rho_c(\tau)], \end{aligned} \tag{B1}$$

where ρ_{st} represents the steady-state density operator of the combined system, and ρ_c represents the conditional state of the combined system, which are prepared by the preselection of mode a on the steady state of the system, that is,

$$\rho_c = a(0)\rho_{st}a^\dagger(0). \tag{B2}$$

At the time range we are concerned with, it can be assumed that mode a is always maintained in vacuum state after preselection, and thus ρ_c can be factorized as

$$\rho_c = \rho_{E,b}^c \otimes \rho_a^c, \tag{B3}$$

where $\rho_a^c = |0_a\rangle\langle 0_a|$ represents the vacuum state of mode a. It can be obtained that the subsystem composed of the emitter and sensor b is in an incoherent superposition state

$$\rho_{E,b}^c(\tau) = |\psi_a(\tau)\rangle\langle\psi_a(\tau)| + |\psi_b(\tau)\rangle\langle\psi_b(\tau)|, \tag{B4}$$

with

$$|\psi_a(\tau)\rangle = \mathcal{C}_{A,0_b}(\tau)|A, 0_b\rangle + \mathcal{C}_{A,1_b}(\tau)|A, 1_b\rangle, \tag{B5}$$

$$|\psi_b(\tau)\rangle = \mathcal{C}_{B,0_b}(\tau)|B, 0_b\rangle + \mathcal{C}_{B,1_b}(\tau)|B, 1_b\rangle. \tag{B6}$$

According to Eqs. (B2) and (B3), we can obtain that the initial conditions of the evolution of the conditional state as

$$\begin{aligned} \mathcal{C}_{A,0_b}(0) &= \mathcal{C}_{A,1_a,0_b}, \\ \mathcal{C}_{A,1_b}(0) &= \mathcal{C}_{A,1_a,1_b}, \\ \mathcal{C}_{B,0_b}(0) &= \mathcal{C}_{B,1_a,0_b}, \\ \mathcal{C}_{B,1_b}(0) &= \mathcal{C}_{B,1_a,1_b}, \end{aligned} \tag{B7}$$

where $\mathcal{C}_{A,1_a,0_b}$, $\mathcal{C}_{A,1_a,1_b}$, $\mathcal{C}_{B,1_a,0_b}$, and $\mathcal{C}_{B,1_a,1_b}$ are the probability amplitudes of the combined system composed of sensors a, b and the emitter under steady-state conditions.

The evolution of $\rho_{E,b}^c$ with the delay τ is determined by

$$\dot{\rho}_{E,b}^c = -i\big[H', \rho_{E,b}^c\big], \tag{B8}$$

with

$$H' = H_b + \big(g_{\pi_1}\sigma_{e_1g_1}b + g_{\pi_2}\sigma_{e_2g_2}b + \mathrm{H.c.}\big), \tag{B9}$$

where $H_b = (\Delta_b - i\frac{\kappa_b}{2})b^\dagger b$ represents the non-Hermitian Hamiltonian of sensor b. The above equation can be easily solved using the perturbation theory, and the analytical expression of the frequency-resolved correlation can be obtained according to Eq. (7). According to the same theoretical method, the analytical expression of the two-photon correlation for the opposite detection ordering can also be obtained.

APPENDIX C: AMPLITUDES OF TWO-PHOTON PATHS

The probability amplitudes of the different spectral components of the two-photon transitions involved in Eqs. (18) and (19) can be expressed as follows.

For the detected frequencies (F^{σ^+}, R^π) shown in Fig. 3(a), the corresponding two-photon emission amplitudes for the detection orderings (a, b) and (b, a) are respectively given by

$$\begin{aligned} &\mathcal{R}[F^{\sigma^+}, R^\pi; \tau] \\ &= -4e^{3i\phi}g_\sigma s_1 s_2\big(g_{\pi_1}c_1 s_1 F^+[\delta_{a,F}, \delta_{b,R}; \delta_{b,R}, \tau] \\ &\quad + g_{\pi_2}c_2 s_2 F^-[\delta_{a,F}, \delta_{b,R}; \delta_{b,R}, \tau]\big), \end{aligned} \tag{C1}$$

$$\begin{aligned} &\mathcal{R}[R^\pi, F^{\sigma^+}; \tau] \\ &= -4e^{3i\phi}g_\sigma s_1 s_2\big(g_{\pi_1}c_1 s_1 F^-[\delta_{b,R}, \delta_{a,F}; \delta_{a,F}, \tau] \\ &\quad + g_{\pi_2}c_2 s_2 F^+[\delta_{b,R}, \delta_{a,F}; \delta_{a,F}, \tau]\big). \end{aligned} \tag{C2}$$

For the detected frequencies (R^{σ^+}, F^π) shown in Fig. 3(b), the corresponding two-photon emission amplitudes for the detection orderings (a, b) and (b, a) are, respectively, given by

$$\begin{aligned} &\mathcal{R}[R^{\sigma^+}, F^\pi; \tau] \\ &= 4e^{3i\phi}g_\sigma s_1 s_2\big(g_{\pi_1}c_1 s_1 F^+\big[\delta_{a,R_1}, \delta_{b,F_1}; \delta_{b,F_1}, \tau\big] \\ &\quad + g_{\pi_2}c_2 s_2 F^-\big[\delta_{a,R_2}, \delta_{b,F_2}; \delta_{b,F_1}, \tau\big]\big), \end{aligned} \tag{C3}$$

$$\mathcal{R}[F^{\pi}, R^{\sigma^+}; \tau] = 4e^{3i\phi} g_\sigma s_1 s_2 \big(g_{\pi_1} c_1 s_1 F^{-}\big[\delta_{b,F_1}, \delta_{a,R_1}; \delta_{a,R_2}, \tau\big] + g_{\pi_2} c_2 s_2 F^{+}\big[\delta_{b,F_2}, \delta_{a,R_2}; \delta_{a,R_2}, \tau\big]\big). \tag{C4}$$

For the detected frequencies (T^{σ^+}, R^{π}) shown in Fig. 3(c), the corresponding two-photon emission amplitudes for the detection orderings (a, b) and (b, a) are respectively given by

$$\mathcal{R}[T^{\sigma^+}, R^{\pi}; \tau] = 4e^{i\phi} g_\sigma c_1 c_2 \big(g_{\pi_1} c_1 s_1 F^{+}[\delta_{a,T}, \delta_{b,R}; \delta_{b,R}, \tau] + g_{\pi_2} c_2 s_2 F^{-}[\delta_{a,T}, \delta_{b,R}; \delta_{b,R}, \tau]\big), \tag{C5}$$

$$\mathcal{R}[R^{\pi}, T^{\sigma^+}; \tau] = 4e^{i\phi} g_\sigma c_1 c_2 \big(g_{\pi_1} c_1 s_1 F^{-}[\delta_{b,R}, \delta_{a,T}; \delta_{a,T}, \tau] + g_{\pi_2} c_2 s_2 F^{+}[\delta_{b,R}, \delta_{a,T}; \delta_{a,T}, \tau]\big). \tag{C6}$$

For the detected frequencies (R^{σ^+}, T^{π}) shown in Fig. 3(d), the corresponding two-photon emission amplitudes for the detection orderings (a, b) and (b, a) are, respectively, given by

$$\mathcal{R}[R^{\sigma^+}, T^{\pi}; \tau] = -4e^{i\phi} g_\sigma c_1 c_2 \big(g_{\pi_1} c_1 s_1 F^{+}[\delta_{a,R_2}, \delta_{b,T_1}; \delta_{b,T_1}, \tau] + g_{\pi_2} c_2 s_2 F^{-}[\delta_{a,R_1}, \delta_{b,T_2}; \delta_{b,T_1}, \tau]\big), \tag{C7}$$

$$\mathcal{R}[T^{\pi}, R^{\sigma^+}; \tau] = -4e^{i\phi} g_\sigma c_1 c_2 \big(g_{\pi_1} c_1 s_1 F^{-}\big[\delta_{b,T_1}, \delta_{a,R_2}, \delta_{a,R_2}, \tau\big] + g_{\pi_2} c_2 s_2 F^{+}\big[\delta_{b,T_2}, \delta_{a,R_1}; \delta_{a,R_2}, \tau\big]\big). \tag{C8}$$

For the detected frequencies (R^{σ^+}, R^{π}) shown in Figs. 3(e) and 3(f), the corresponding two-photon emission amplitudes for the detection orderings (a, b) and (b, a) are, respectively, given by

$$\mathcal{R}_1[R^{\sigma^+}, R^{\pi}; \tau] = 4e^{2i\phi} g_\sigma c_1 s_2 \big(g_{\pi_1} c_1 s_1 F^{+}\big[\delta_{a,R_1}, \delta_{b,R}; \delta_{b,R}, \tau\big] - g_{\pi_2} c_2 s_2 F^{-}\big[\delta_{a,R_1}, \delta_{b,R}; \delta_{b,R}, \tau\big]\big), \tag{C9}$$

$$\mathcal{R}_1[R^{\pi}, R^{\sigma^+}; \tau] = 4e^{2i\phi} g_\sigma c_1 s_2 \big(g_{\pi_1} c_1 s_1 F^{-}\big[\delta_{b,R}, \delta_{a,R_1}; \delta_{a,R_1}, \tau\big] - g_{\pi_2} c_2 s_2 F^{+}\big[\delta_{b,R}, \delta_{a,R_1}; \delta_{a,R_1}, \tau\big]\big), \tag{C10}$$

$$\mathcal{R}_2[R^{\sigma^+}, R^{\pi}; \tau] = 4e^{2i\phi} g_\sigma c_2 s_1 \big(-g_{\pi_1} c_1 s_1 F^{+}\big[\delta_{a,R_2}, \delta_{b,R}; \delta_{b,R}, \tau\big] + g_{\pi_2} c_2 s_2 F^{-}\big[\delta_{a,R_2}, \delta_{b,R}; \delta_{b,R}, \tau\big]\big), \tag{C11}$$

$$\mathcal{R}_2[R^{\pi}, R^{\sigma^+}; \tau] = 4e^{2i\phi} g_\sigma c_2 s_1 \big(-g_{\pi_1} c_1 s_1 F^{-}\big[\delta_{b,R}, \delta_{a,R_2}; \delta_{a,R_2}, \tau\big] + g_{\pi_2} c_2 s_2 F^{+}\big[\delta_{b,R}, \delta_{a,R_2}; \delta_{a,R_2}, \tau\big]\big), \tag{C12}$$

where Eqs. (C9) and (C10) are corresponding to the amplitudes of the two-photon transitions shown in Fig. 3(e), and Eqs. (C11) and (C12) are corresponding to the amplitudes of the two-photon transitions shown in Fig. 3(f).

For the detected frequencies (F^{σ^+}, T^{π}) shown in Figs. 3(g) and 3(h), the corresponding two-photon emission amplitudes for the detection orderings (a, b) and (b, a) are, respectively, given by

$$\mathcal{R}_1[F^{\sigma^+}, T^{\pi}; \tau] = -4e^{2i\phi} g_\sigma g_{\pi_1} c_1^2 s_1 s_2 F^{+}\big[\delta_{a,F}, \delta_{b,T_1}; \delta_{b,T_1}, \tau\big], \tag{C13}$$

$$\mathcal{R}_1[T^{\pi}, F^{\sigma^+}; \tau] = -4e^{2i\phi} g_\sigma g_{\pi_1} c_1^2 s_1 s_2 F^{-}\big[\delta_{b,T_1}, \delta_{a,F}; \delta_{a,R_1}, \tau\big], \tag{C14}$$

$$\mathcal{R}_2[F^{\sigma^+}, T^{\pi}; \tau] = -4e^{2i\phi} g_\sigma g_{\pi_2} c_2^2 s_1 s_2 F^{-}\big[\delta_{a,F}, \delta_{b,T_2}; \delta_{b,R}, \tau\big], \tag{C15}$$

$$\mathcal{R}_2[T^{\pi}, F^{\sigma^+}; \tau] = -4e^{2i\phi} g_\sigma g_{\pi_2} c_2^2 s_1 s_2 F^{+}\big[\delta_{b,T_2}, \delta_{a,F}; \delta_{a,F}, \tau\big], \tag{C16}$$

where Eqs. (C13) and (C14) correspond to the amplitudes of the two-photon transitions shown in Fig. 3(g), and Eqs. (C15) and (C16) correspond to the amplitudes of the two-photon transitions shown in Fig. 3(h).

For the detected frequencies (T^{σ^+}, F^{π}) shown in Figs. 3(i) and 3(j), the corresponding two-photon emission amplitudes for the detection orderings (a, b) and (b, a) are, respectively, given by

$$\mathcal{R}_1[T^{\sigma^+}, F^{\pi}; \tau] = 4e^{2i\phi} g_\sigma g_{\pi_1} c_1 c_2 s_1^2 F^{+}\big[\delta_{a,T}, \delta_{b,F_1}; \delta_{b,F_1}, \tau\big], \tag{C17}$$

$$\mathcal{R}_1[F^{\pi}, T^{\sigma^+}; \tau] = 4e^{2i\phi} g_\sigma g_{\pi_1} c_1 c_2 s_1^2 F^{-}\big[\delta_{b,F_1}, \delta_{a,T}; \delta_{a,R_2}, \tau\big], \tag{C18}$$

$$\mathcal{R}_2[T^{\sigma^+}, F^{\pi}; \tau] = 4e^{2i\phi} g_\sigma g_{\pi_2} c_1 c_2 s_2^2 F^{-}\big[\delta_{a,T}, \delta_{b,F_2}; \delta_{b,R}, \tau\big], \tag{C19}$$

$$\mathcal{R}_2[F^{\pi}, T^{\sigma^+}; \tau] = 4e^{2i\phi} g_\sigma g_{\pi_2} c_1 c_2 s_2^2 F^{+}\big[\delta_{b,F_2}, \delta_{a,T}; \delta_{a,T}, \tau\big], \tag{C20}$$

where Eqs. (C17) and (C18) are corresponding to the amplitudes of the two-photon transitions shown in Fig. 3(i), and Eqs. (C19) and (C20) are corresponding to the amplitudes of the two-photon transitions shown in Fig. 3(j).

APPENDIX D: AVERAGE POPULATIONS OF SENSORS

Under the parameter condition introduced in Sec. III (i.e., $\Omega \gg \kappa \gg \gamma$), the average populations of the sensors in a steady-state condition can be analytically solved using the perturbation theory. Therefore, the average population of sensor a is given by

$$\langle n_a \rangle = \langle n_{a,F} \rangle + \langle n_{a,R} \rangle + \langle n_{a,T} \rangle. \tag{D1}$$

Here $\langle n_{a,F}\rangle$, $\langle n_{a,R}\rangle$, and $\langle n_{a,T}\rangle$, respectively, correspond to the contributions of the F, R, and T lines in σ^+ transition, and the explicit expressions are given by

$$\langle n_{a,F}\rangle = \frac{g_\sigma^2 s_1^2 s_2^2 \rho_{CC}}{(E_B - E_C + \Delta_a)^2 + \left(\frac{\kappa_a}{2}\right)^2}, \tag{D2}$$

$$\langle n_{a,R}\rangle = \frac{g_\sigma^2 c_1^2 s_2^2 \rho_{CC}}{(E_A - E_C + \Delta_a)^2 + \left(\frac{\kappa_a}{2}\right)^2} + \frac{g_\sigma^2 c_2^2 s_1^2 \rho_{DD}}{(E_B - E_D + \Delta_a)^2 + \left(\frac{\kappa_a}{2}\right)^2}, \tag{D3}$$

$$\langle n_{a,T}\rangle = \frac{g_\sigma^2 c_1^2 c_2^2 \rho_{DD}}{(E_A - E_D + \Delta_a)^2 + \left(\frac{\kappa_a}{2}\right)^2}. \tag{D4}$$

Similarly, the average population of sensor b is given by

$$\langle n_b\rangle = \langle n_{b,F}\rangle + \langle n_{b,R}\rangle + \langle n_{b,T}\rangle. \tag{D5}$$

Here $n_{b,F}$, $n_{b,R}$, and $n_{b,T}$, respectively, correspond to the contributions of the F, R, and T lines in π transition, and the explicit expressions are given by

$$\langle n_{b,F}\rangle = \frac{g_{\pi_1}^2 s_1^4 \rho_{AA}}{(E_B - E_A + \Delta_b)^2 + \left(\frac{\kappa_b}{2}\right)^2} + \frac{g_{\pi_2}^2 s_2^4 \rho_{CC}}{(E_D - E_C + \Delta_b)^2 + \left(\frac{\kappa_b}{2}\right)^2}, \tag{D6}$$

$$\langle n_{b,R}\rangle = \frac{g_{\pi_1}^2 c_1^2 s_1^2 (\rho_{AA} + \rho_{BB})}{\Delta_b^2 + \left(\frac{\kappa_b}{2}\right)^2} + \frac{g_{\pi_2}^2 c_2^2 s_2^2 (\rho_{CC} + \rho_{DD})}{\Delta_b^2 + \left(\frac{\kappa_b}{2}\right)^2}, \tag{D7}$$

$$\langle n_{b,F}\rangle = \frac{g_{\pi_1}^2 s_1^4 \rho_{BB}}{(E_B - E_A + \Delta_b)^2 + \left(\frac{\kappa_b}{2}\right)^2} + \frac{g_{\pi_2}^2 s_2^4 \rho_{CC}}{(E_D - E_C + \Delta_b)^2 + \left(\frac{\kappa_b}{2}\right)^2}. \tag{D8}$$

[1] G. S. Agarwal, *Quantum Statistical Theories of Spontaneous Emission and Their Relation to Other Approaches*, Springer Tracts in Modern Physics: Quantum Optics (Springer-Verlag, Berlin, 1974), p. 94.
[2] Z. Ficek and S. Swain, J. Mod. Opt. **49**, 3 (2002).
[3] P. Zhou and S. Swain, Phys. Rev. Lett. **77**, 3995 (1996); Phys. Rev. A **56**, 3011 (1997).
[4] S. Y. Gao, F. L. Li, and S. Y. Zhu, Phys. Rev. A **66**, 043806 (2002).
[5] I. Gonzalo, M. A. Antón, F. Carreño, and O. G. Calderón, Phys. Rev. A **72**, 033809 (2005).
[6] M. Fleischhauer, C. H. Keitel, L. M. Narducci, M. O. Scully, S. Y. Zhu, and M. S. Zubairy, Opt. Commun. **94**, 599 (1992).
[7] H.-R. Xia, C.-Y. Ye, and S.-Y. Zhu, Phys. Rev. Lett. **77**, 1032 (1996).
[8] M. V. Gurudev Dutt, J. Cheng, B. Li, X. Xu, X. Li, P. R. Berman, D. G. Steel, A. S. Bracker, D. Gammon, S. E. Economou, R.-B. Liu, and L. J. Sham, Phys. Rev. Lett. **94**, 227403 (2005).
[9] K. P. Heeg, H. C. Wille, K. Schlage, T. Guryeva, D. Schumacher, I. Uschmann, K. S. Schulze, B. Marx, T. Kämpfer, G. G. Paulus, R. Röhlsberger, and J. Evers, Phys. Rev. Lett. **111**, 073601 (2013).
[10] Y. He, Y.-M. He, J. Liu, Y.-J. Wei, H. Y. Ramírez, M. Atatüre, C. Schneider, M. Kamp, S. Höfling, C.-Y. Lu, and J.-W. Pan, Phys. Rev. Lett. **114**, 097402 (2015).
[11] M. Kiffner, J. Evers, and C. H. Keitel, Phys. Rev. Lett. **96**, 100403 (2006); Phys. Rev. A **73**, 063814 (2006).
[12] S. Das and G. S. Agarwal, Phys. Rev. A **77**, 033850 (2008).
[13] U. Eichmann, J. C. Bergquist, J. J. Bollinger, J. M. Gilligan, W. M. Itano, D. J. Wineland, and M. G. Raizen, Phys. Rev. Lett. **70**, 2359 (1993).
[14] U. Dorner and P. Zoller, Phys. Rev. A **66**, 023816 (2002).
[15] F. Dubin, D. Rotter, M. Mukherjee, C. Russo, J. Eschner, and R. Blatt, Phys. Rev. Lett. **98**, 183003 (2007).
[16] R. J. Glauber, Phys. Rev. Lett. **10**, 84 (1963).
[17] R. J. Glauber, Phys. Rev. **130**, 2529 (1963).
[18] C. Cohen-Tannoudji and S. Reynaud, Philos. Trans. R. Soc. London, Ser. A **293**, 223 (1979).
[19] J. Dalibard and S. Reynaud, J. Phys. (Paris) **44**, 1337 (1983).
[20] L. Knöll and G. Weber, J. Phys. B **19**, 2817 (1986).
[21] G. Nienhuis, Phys. Rev. A **47**, 510 (1993).
[22] E. del Valle, A. Gonzalez-Tudela, F. P. Laussy, C. Tejedor, and M. J. Hartmann, Phys. Rev. Lett. **109**, 183601 (2012).
[23] A. González-Tudela, F. P. Laussy, C. Tejedor, M. J. Hartmann, and E. del Valle, New J. Phys. **15**, 033036 (2013).
[24] B. Silva, C. Sánchez Muñoz, D. Ballarini, A. González-Tudela, M. de Giorgi, G. Gigli, K. West, L. Pfeiffer, E. del Valle, D. Sanvitto, and F. P. Laussy, Sci. Rep. **6**, 37980 (2016).
[25] M. Peiris, B. Petrak, K. Konthasinghe, Y. Yu, Z. C. Niu, and A. Muller, Phys. Rev. B **91**, 195125 (2015).
[26] M. Peiris, K. Konthasinghe, and A. Muller, Phys. Rev. Lett. **118**, 030501 (2017).
[27] C. Sánchez Muñoz, E. del Valle, C. Tejedor, and F. P. Laussy, Phys. Rev. A **90**, 052111 (2014).
[28] E. del Valle, New J. Phys. **15**, 025019 (2013).
[29] F. P. Laussy, Nat. Mater. **16**, 398 (2017).
[30] J. D. Cresser, J. Phys. B **20**, 4915 (1987).
[31] N. Akopian, N. H. Lindner, E. Poem, Y. Berlatzky, J. Avron, D. Gershoni, B. D. Gerardot, and P. M. Petroff, Phys. Rev. Lett. **96**, 130501 (2006).
[32] K. Hennessy, A. Badolato, M. Winger, D. Gerace, M. Atature, S. Gulde, S. Fält, E. L. Hu, and A. Imamoğlu, Nature (London) **445**, 896 (2007).
[33] M. Kaniber, A. Laucht, A. Neumann, J. M. Villas-Bôas, M. Bichler, M.-C. Amann, and J. J. Finley, Phys. Rev. B **77**, 161303(R) (2008).
[34] G. Sallen, A. Tribu, T. Aichele, R. André, L. Besombes, C. Bougerol, M. Richard, S. Tatarenko, K. Kheng, and J.-Ph. Poizat, Nat. Photonics **4**, 696 (2010).
[35] A. Ulhaq, S. Weiler, S. M. Ulrich, R. Roßbach, M. Jetter, and P. Michler, Nat. Photonics **6**, 238 (2012).
[36] Y. Nieves and A. Muller, Phys. Rev. B **98**, 165432 (2018).

[37] C. Dory, K. A. Fischer, K. Müller, K. G. Lagoudakis, T. Sarmiento, A. Rundquist, J. L. Zhang, Y. Kelaita, N. V. Sapra, and J. Vučković, Phys. Rev. A **95**, 023804 (2017).
[38] K. E. Dorfman and S. Mukamel, Proc. Natl. Acad. Sci. USA **115**, 1451 (2018).
[39] J. Canet-Ferrer, R. García-Calzada, J. P. Martínez-Pastor, and G. Muñoz-Matutano, ACS Photonics **6**, 181 (2019).
[40] P. G. Kwiat, K. Mattle, H. Weinfurter, A. Zeilinger, A. V. Sergienko, and Y. Shih, Phys. Rev. Lett. **75**, 4337 (1995).
[41] P. Kolchin, S. Du, C. Belthangady, G. Y. Yin, and S. E. Harris, Phys. Rev. Lett. **97**, 113602 (2006).
[42] A. Aspect, J. Dalibard, and G. Roger, Phys. Rev. Lett. **49**, 1804 (1982).
[43] R. J. Young, R. M. Stevenson, P. Atkinson, K. Cooper, D. A. Ritchie, and A. J. Shields, New J. Phys. **8**, 29 (2006).
[44] L.-M. Duan, M. D. Lukin, J. I. Cirac, and P. Zoller, Nature (London) **414**, 413 (2001).
[45] P. Kok, W. J. Munro, K. Nemoto, T. C. Ralph, J. P. Dowling, and G. J. Milburn, Rev. Mod. Phys. **79**, 135 (2007).
[46] H. J. Kimble, Nature (London) **453**, 1023 (2008).
[47] W. Yao, R.-B. Liu, and L. J. Sham, Phys. Rev. Lett. **95**, 030504 (2005).
[48] C. A. Schrama, G. Nienhuis, H. A. Dijkerman, C. Steijsiger, and H. G. M. Heideman, Phys. Rev. Lett. **67**, 2443 (1991); Phys. Rev. A **45**, 8045 (1992).
[49] Z. A. Peng, G. Q. Yang, Q. L. Wu, and G. X. Li, Phys. Rev. A **98**, 043828 (2018).
[50] T. M. Stace, G. J. Milburn, and C. H. W. Barnes, Phys. Rev. B **67**, 085317 (2003).
[51] S. Schumacher, J. Förstner, A. Zrenner, M. Florian, C. Gies, P. Gartner, and F. Jahnke, Opt. Express **20**, 5335 (2012).
[52] E. A. Meirom, N. H. Lindner, Y. Berlatzky, E. Poem, N. Akopian, J. E. Avron, and D. Gershoni, Phys. Rev. A **77**, 062310 (2008).
[53] D. M. Brink and G. R. Satchler, *Angular Momentum*, 3rd ed. (Clarendon, Oxford, 1994).
[54] J. L. Meunier, Eur. Phys. J. **8**, 114 (1987).
[55] M. Auzinsh, D. Budker, and S. M. Rochester, *Optically Polarized Atoms: Understanding Light-Atom Interactions*, 1st ed. (Oxford University Press, Oxford, 2010).